High-Spin Mn 4 and Mn 10 Molecules: Large Spin Changes with Structure in Mixed-Valence Mn II 4 Mn III 6 Clusters with Azide and Alkoxide-Based Ligands

ARTICLE *in* INORGANIC CHEMISTRY · JULY 2008

Impact Factor: 4.76 · DOI: 10.1021/ic800268z · Source: PubMed

6 AUTHORS, INCLUDING:

Theocharis C Stamatatos
University of Patras
143 PUBLICATIONS **3,615** CITATIONS
SEE PROFILE

Khalil Abboud
University of Florida
580 PUBLICATIONS **12,507** CITATIONS
SEE PROFILE

Wolfgang Wernsdorfer
French National Centre for Scientific Resea…
611 PUBLICATIONS **31,930** CITATIONS
SEE PROFILE

George Christou
University of Florida
757 PUBLICATIONS **28,995** CITATIONS
SEE PROFILE

Inorg. Chem. **2008**, *47*, 5006−5021

High-Spin Mn_4 and Mn_{10} Molecules: Large Spin Changes with Structure in Mixed-Valence $Mn^{II}_4Mn^{III}_6$ Clusters with Azide and Alkoxide-Based Ligands

Theocharis C. Stamatatos,[†] Katye M. Poole,[‡] Khalil A. Abboud,[†] Wolfgang Wernsdorfer,[§] Ted A. O'Brien,[‡] and George Christou*,[†]

Department of Chemistry, University of Florida, Gainesville, Florida 32611-7200, Institut Néel-CNRS, BP-166 Grenoble, 25 Avenue des Martyrs, 38042 Grenoble, Cedex 9, France, and Department of Chemistry and Chemical Biology, Indiana University-Purdue University Indianapolis, Indianapolis, Indiana 46202-3274

Received February 12, 2008

The use has been explored of both azide (N_3^-) and alkoxide-containing groups such as the anions of 2-(hydroxymethyl)pyridine (hmpH), 2,6-pyridinedimethanol ($pdmH_2$), 1,1,1-tris(hydroxymethyl)ethane ($thmeH_3$) and triethanolamine ($teaH_3$) in Mn cluster chemistry. The 1:1:1:1 reactions of hmpH, NaN_3 and NEt_3 with $Mn(ClO_4)_2 \cdot 6H_2O$ or $Mn(NO_3)_2 \cdot H_2O$ in MeCN/MeOH afford $[Mn^{II}_4Mn^{III}_6O_4(N_3)_4(hmp)_{12}](X)_2$ [X = ClO_4^- (**1**), N_3^- (**2**)]. The $[Mn_{10}(\mu_4\text{-}O)_4(\mu_3\text{-}N_3)_4]^{14+}$ core of the cation has a tetra-face-capped octahedral topology, with a central Mn^{III}_6 octahedron, whose eight faces are bridged by four μ_3-N_3^- and four μ_4-O^{2-} ions, the latter also bridging to four extrinsic Mn^{II} atoms. The core has T_d symmetry, but the complete $[Mn^{II}_4Mn^{III}_6O_4(N_3)_4(hmp)_{12}]^{2+}$ cation has rare *T* symmetry, which is crystallographically imposed. A similar reaction of $Mn(ClO_4)_2 \cdot 6H_2O$ with one equiv each of NaN_3, $thmeH_3$, $pdmH_2$, and NEt_3 in MeCN/MeOH led to $[Mn^{II}_4Mn^{III}_6O_2(N_3)_6(pdmH)_4(thme)_4]$ (**3**). Complex **3** is at the same oxidation level as **1**/**2** but its core is structurally different, consisting of two edge-fused $[Mn^{II}_2Mn^{III}_4(\mu_4\text{-}O)]^{14+}$ octahedra. Replacement of $thmeH_3$ with $teaH_3$ in this reaction gave instead $[Mn^{II}_2Mn^{III}_2(N_3)_4(pdmH)_2(teaH)_2]$ (**4**), containing a planar Mn_4 rhombus. Variable-temperature, solid-state dc and ac magnetization studies were carried out on **1**−**4** in the 5.0–300 K range. Complexes **1** and **2** are completely ferromagnetically coupled with a resulting $S = 22$ ground state, one of the highest yet reported. Fits of dc magnetization vs field (*H*) and temperature (*T*) data by matrix diagonalization gave $S = 22$, $g = 2.00$, and $D \approx 0.0$ cm^{-1} (*D* is the axial zero-field splitting parameter). In contrast, the data for **3** revealed dominant antiferromagnetic interactions and a resulting $S = 0$ ground state. Complex **4** contains weakly ferromagnetically coupled Mn atoms, leading to an $S = 9$ ground-state and low-lying excited states, and exhibits out-of-phase ac susceptibility signals characteristic of a single-molecule magnet. Theoretical values of the exchange constants in **1** obtained with density functional theory and ZILSH calculations were in good agreement with experimental values. The combined work demonstrates the synthetic usefulness of alcohol-based chelates and azido ligands when used together, and the synthesis in the present work of two "isomeric" $Mn^{III}_6Mn^{II}_4$ cores that differ in spin by a remarkable 22 units.

Introduction

The continuing interest in the synthesis and characterization of polynuclear manganese complexes in intermediate oxidation states derives mainly from their relevance to two fields. First, the ability of Mn to exist in a number of oxidation states (II−IV) under normal conditions has induced the desire to recreate with synthetic models the structure, spectroscopic properties, and/or function of the active sites of several redox enzymes; the most fascinating of these is the water-oxidizing complex (WOC) of green plants and cyanobacteria, which is a Mn_4Ca complex.[1,2] Second, oligo- and polynuclear Mn compounds containing Mn^{III} atoms have been found to often have large, and sometimes abnormally large, ground-state spin (*S*) values, which combined with a large and negative magnetoanisotropy (as reflected in a large

* To whom correspondence should be addressed. E-mail: christou@chem.ufl.edu.
[†] University of Florida.
[‡] Indiana University-Purdue University Indianapolis.
[§] Institut Néel-CNRS.

10.1021/ic800268z CCC: $40.75
Published on Web 05/03/2008

and negative zero-field splitting parameter, D) have led to some of these species functioning as single-molecule magnets (SMMs).[3] SMMs have a significant energy barrier (vs kT, where k is the Boltzmann constant) to magnetization relaxation and thus, at sufficiently low temperatures, will function as nanoscale magnetic particles.[4] In addition, they display quantum effects such as quantum tunneling of the magnetization (QTM)[5] and quantum phase interference.[6] The upper limit to the barrier (U) is given by $S^2|D|$ or $(S^2 - 1/4)|D|$ for integer and half-integer spin, respectively. However, in practice, QTM through upper regions of the anisotropy barrier via higher lying M_s levels of the spin S manifold results in the actual or effective barrier (U_{eff}) being less than U.[3,5]

There is thus a continuing interest in the general challenge of developing synthetic procedures to new high-spin molecules from simple reagents, whether for SMM applications or not. The latter depends on the magnitude of the anisotropy parameter, D, and recent examples of complexes with large S but small D include $Mn_{28}Cu_{17}$, Mn_{25}, and Mn_{19} complexes with $S = 51/2$,[7] $51/2$[8] and $61/2$,[9] and $83/2$[10] ground states, respectively.

Various procedures to high-spin molecules have been reported to date.[7−14] In the present study, we have sought to extend our previous work where we had employed both azide groups and alkoxide-based chelates in Mn reactions, and had obtained interesting new complexes with high S values;[8,15] the same strategy has since also been employed successfully by others.[10,16] The azide (N_3^-) group bridging metal ions in the 1,1- (end-on) fashion is a mediator of ferromagnetic exchange coupling for a wide range of M−N−M angles and has thus found widespread utility in molecular chemistry for this purpose,[17,18] as well as in 1-, 2- or 3D extended networks.[19] However, only very recently has it found employment in high nuclearity Mn^{III}-containing cluster chemistry.[8,10,15,16] Similarly, we and others have had a longstanding interest in the use of alkoxide-based chelating ligands such as the anions of 2-(hydroxymethyl)pyridine (hmpH)[9,15,20] and 2,6-pyridinedimethanol ($pdmH_2$)[8,21] in Mn cluster chemistry. These and related ones such as the anions of 1,1,1-tris(hydroxymethyl)ethane ($thmeH_3$),[22] triethanolamine ($teaH_3$),[23] *N*-methyldiethanolamine ($mdaH_2$),[24] and others are excellent bridging units that can foster formation of high nuclearity products. From a magnetic point of view, their alkoxide arm(s) often support ferromagnetic coupling

(1) (a) Ferreira, K. N.; Iverson, T. M.; Maghlaoui, K.; Barber, J.; Iwata, S. *Science* **2004**, *303*, 1831. (b) Carrell, T. G.; Tyryshkin, A. M.; Dismukes, G. C. *J. Biol. Inorg. Chem.* **2002**, *7*, 2. (c) Cinco, R. M.; Rompel, A.; Visser, H.; Aromi, G.; Christou, G.; Sauer, K.; Klein, M. P.; Yachandra, V. K. *Inorg. Chem.* **1999**, *38*, 5988. (d) Yachandra, V. K.; Sauer, K.; Klein, M. P. *Chem. Rev.* **1996**, *96*, 2927.

(2) (a) Law, N. A.; Caudle, M. T.; Pecoraro, V. L. In *Advances in Inorganic Chemistry*; Sykes, A. G.; Ed.; Academic Press: London, 1998; Vol. *46*, p 305. (b) Yocum, C. F.; Pecoraro, V. L. *Curr. Opin. Chem. Biol.* **1999**, *3*, 182.

(3) For some representative references, see :(a) Christou, G.; Gatteschi, D.; Hendrickson, D. N.; Sessoli, R. *MRS Bull.* **2000**, *25*, 66. (b) Sessoli, R.; Tsai, H.-L.; Schake, A. R.; Wang, S.; Vincent, J. B.; Folting, K.; Gatteschi, D.; Christou, G.; Hendrickson, D. N. *J. Am. Chem. Soc.* **1993**, *115*, 1804.

(4) (a) Bircher, R.; Chaboussant, G.; Dobe, D.; Güdel, H. U.; Oshsenbein, S. T.; Sieber, A.; Waldmann, O. *Adv. Funct. Mater.* **2006**, *16*, 209. (b) Gatteschi, D.; Sessoli, R. *Angew. Chem., Int. Ed.* **2003**, *42*, 268. (c) Aubin, S. M. J.; Gilley, N. R.; Pardi, L.; Krzystek, J.; Wemple, M. W.; Brunel, L.- C.; Maple, M. B.; Christou, G.; Hendrickson, D. N. *J. Am. Chem. Soc.* **1998**, *120*, 4991. (d) Oshio, H.; Nakano, M. *Chem.—Eur. J.* **2005**, *11*, 5178.

(5) (a) Friedman, J. R.; Sarachik, M. P. *Phys. Rev. Lett.* **1996**, *76*, 3830. (b) Thomas, L.; Lionti, L.; Ballou, R.; Gatteschi, D.; Sessoli, R.; Barbara, B. *Nature* **1996**, *383*, 145.

(6) (a) Wernsdorfer, W.; Sessoli, R. *Science* **2000**, 2417. (b) Wernsdorfer, W.; Soler, M.; Christou, G.; Hendrickson, D. N. *Phys. Rev. Lett.* **2005**, *95*, 037203 (1-4). (c) Wernsdorfer, W.; Chakov, N. E.; Christou, G. *Phys. Rev. Lett.* **2005**, *95*–4)

(7) Wang, W.- G.; Zhou, A.- J.; Zhang, W.- X.; Tong, M.- L.; Chen, X.- M.; Nakano, M.; Beedle, C. C.; Hendrickson, D. N. *J. Am. Chem. Soc.* **2007**, *129*, 1014.

(8) Murugesu, M.; Habrych, M.; Wernsdorfer, W.; Abboud, K. A.; Christou, G. *J. Am. Chem. Soc.* **2004**, *126*, 4766.

(9) Stamatatos, Th. C.; Abboud, K. A.; Wernsdorfer, W.; Christou, G. *Angew. Chem., Int. Ed.* **2007**, *46*, 884.

(10) Ako, A. M.; Hewitt, I. J.; Mereacre, V.; Clérac, R.; Wernsdorfer, W.; Anson, C. E.; Powell, A. K. *Angew. Chem., Int. Ed.* **2006**, *45*, 4926.

(11) Christou, G. *Polyhedron* **2005**, *24*, 2065; and references therein.

(12) (a) Boudalis, A. K.; Donnadieu, B.; Nastopoulos, V.; Clemente-Juan, J. M.; Mari, A.; Sanakis, Y.; Tuchagues, J.- P.; Perlepes, S. P. *Angew. Chem., Int. Ed.* **2004**, *43*, 2266. (b) Papaefstathiou, G. S.; Perlepes, S. P.; Escuer, A.; Vicente, R.; Font-Bardia, M.; Solans, X. *Angew. Chem., Int. Ed.* **2001**, *40*, 884. (c) Papaefstathiou, G. S.; Escuer, A.; Vicente, R.; Font-Bardia, M.; Solans, X.; Perlepes, S. P. *Chem. Commun.* **2001**, 2414.

(13) (a) Zhao, H.; Shatruk, M.; Prosvirin, A. V.; Dunbar, K. R. *Chem.—Eur. J.* **2007**, *13*, 6573. (b) Schelter, E. J.; Karadas, F.; Avendano, C.; Prosvirin, A. V.; Wernsdorfer, W.; Dunbar, K. R. *J. Am. Chem. Soc.* **2007**, *129*, 8139. (c) Aromi, G.; Brechin, E. K. *Struct. Bonding (Berlin)* **2006**, *122*, 1; and references therein.

(14) (a) Harris, T. D.; Long, J. R. *Chem. Commun.* **2007**, 1360. (b) Wang, S.; Zuo, J.- L.; Zhou, H.- C.; Choi, H. J.; He, Y.; Long, J. R.; You, X.- Z. *Angew. Chem., Int. Ed.* **2004**, *43*, 5940. (c) Wang, C.-F.; Zuo, J.-L.; Bartlett, B. M.; Song, Y.; Long, J. R.; You, X.-Z. *J. Am. Chem. Soc.* **2006**, *128*, 7162.

(15) (a) Stamatatos, Th. C.; Abboud, K. A.; Wernsdorfer, W.; Christou, G. *Angew. Chem., Int. Ed.* **2006**, *45*, 4134. (b) Stamatatos, Th. C.; Abboud, K. A.; Wernsdorfer, W.; Christou, G. *Polyhedron* **2007**, *26*, 2042.

(16) (a) Scott, R. T. W.; Milios, C. J.; Vinslava, A.; Lifford, D.; Parsons, S.; Wernsdorfer, W.; Christou, G.; Brechin, E. K. *Dalton Trans.* **2006**, 3161. (b) Scott, R. T. W.; Parsons, S.; Murugesu, M.; Wernsdorfer, W.; Christou, G.; Brechin, E. K. *Angew. Chem., Int. Ed.* **2005**, 6540.

(17) Kahn, O. *Molecular Magnetism*; VCH Publishers: New York, 1993.

(18) (a) Escuer, A.; Aromi, G. *Eur. J. Inorg. Chem.* **2006**, 4721; and references therein. (b) Ruiz, E.; Cano, J.; Alvarez, S.; Alemany, P. *J. Am. Chem. Soc.* **1998**, *120*, 11122.

(19) For a representative review, see Ribas, J.; Escuer, A.; Monfort, M.; Vicente, R.; Cortes, R.; Lezama, L.; Rojo, T. *Coord. Chem. Rev.* **1999**, *193–195*, 1027; and references therein.

(20) (a) Harden, N. C.; Bolcar, M. A.; Wernsdorfer, W.; Abboud, K. A.; Streib, W. E.; Christou, G. *Inorg. Chem.* **2003**, *42*, 7067. (b) Yang, E.- C.; Harden, N.; Wernsdorfer, W.; Zakharov, L.; Brechin, E. K.; Rheingold, A. L.; Christou, G.; Hendrickson, D. N. *Polyhedron* **2003**, *22*, 1857. (c) Boskovic, C.; Brechin, E. K.; Streib, W. E.; Folting, K.; Bollinger, J. C.; Hendrickson, D. N.; Christou, G. *J. Am. Chem. Soc.* **2002**, *124*, 3725. (d) Lecren, L.; Roubeau, O.; Coulon, C.; Li, Y.- G.; Goff, X. F. L.; Wernsdorfer, W.; Miyasaka, H.; Clérac, R. *J. Am.Chem. Soc.* **2005**, *127*, 17353. (e) Lecren, L.; Wernsdorfer, W.; Li, Y.- G.; Roubeau, O.; Miyasaka, H.; Clérac, R. *J. Am. Chem. Soc.* **2005**, *127*, 11311.

(21) (a) Boskovic, C.; Wernsdorfer, W.; Folting, K.; Huffman, J. C.; Hendrickson, D. N.; Christou, G. *Inorg. Chem.* **2002**, *41*, 5107. (b) Brechin, E. K.; Yoo, J.; Huffman, J. C.; Hendrickson, D. N.; Christou, G. *Chem. Commun.* **1999**, 783. (c) Murugesu, M.; Wernsdorfer, W.; Abboud, K. A.; Christou, G. *Polyhedron* **2005**, *24*, 2894. (d) Miyasaka, H.; Nakata, K.; Lecren, L.; Coulon, C.; Nakazawa, Y.; Fujisaki, T.; Sugiura, K.; Yamashita, M.; Clérac, R. *J. Am.Chem. Soc.* **2006**, *128*, 3770. (e) Murugesu, M.; Mishra, A.; Wernsdorfer, W.; Abboud, K. A.; Christou, G. *Polyhedron* **2006**, *25*, 613.

(22) For a representative review, see Brechin, E. K. *Chem. Commun.* **2005**, 5141; and references therein.

(23) (a) Murugesu, M.; Wernsdorfer, W.; Abboud, K. A.; Christou, G. *Angew. Chem., Int. Ed.* **2005**, *44*, 892; and references therein. (b) Stamatatos, Th. C.; Abboud, K. A.; O'Brien, T. A.; Wernsdorfer, W.; Christou, G., unpublished results.

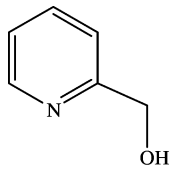

hmpH

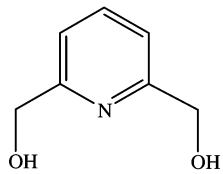

$pdmH_2$

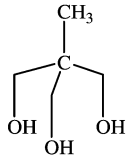

$thmeH_3$

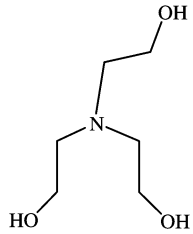

$teaH_3$

between the metal atoms that they bridge.[8,9,15,20a,b,21a,25] These facts stimulated us to further explore mixed azide/alkoxide-chelate reaction systems in Mn chemistry as a potential route to new high spin cluster compounds. We herein report the results from our investigation of the use of N_3^-/hmp$^-$, N_3^-/thme^{3-}/pdmH$^-$ and N_3^-/teaH^{2-}/pdmH$^-$ combinations in certain Mn noncarboxylate reactions. These reaction systems have led to two new types of mixed-valence Mn_{10} products, $[Mn^{II}_4Mn^{III}_6O_4(N_3)_4(hmp)_{12}](X)_2$ [X = ClO_4^- (**1**), N_3^- (**2**)] and $[Mn^{II}_4Mn^{III}_6O_2(N_3)_6(pdmH)_4(thme)_4]$ (**3**), respectively, with completely different structural and magnetic properties, as well as a new, ferromagnetically coupled, mixed-valence $[Mn^{II}_2Mn^{III}_2(N_3)_4(pdmH)_2(teaH)_2]$ (**4**) cluster which shows strongly the slow relaxation of magnetization. Portions of this work have been previously communicated.[15]

Experimental Section

Syntheses. All manipulations were performed under aerobic conditions using materials as received. ***Caution!*** *Although no such behavior was observed during the present work, perchlorate and azide salts are potentially explosive; such compounds should be synthesized and used in small quantities, and treated with utmost care at all times.*

$[Mn_{10}O_4(N_3)_4(hmp)_{12}](ClO_4)_2$ (1). To a stirred solution of hmpH (0.19 mL, 2.0 mmol) and NEt_3 (0.28 mL, 2.0 mmol) in MeCN/MeOH (20/2 mL) was added solid NaN_3 (0.13 g, 2.0 mmol). The mixture was stirred for a further 15 min and then solid $Mn(ClO_4)_2\cdot 6H_2O$ (0.72 g, 2.0 mmol) was added under vigorous stirring, which caused a rapid color change from pale yellow to dark brown. The solution was stirred for a further 2 h, filtered, and the filtrate left undisturbed at ambient temperature. After 3 days, X-ray quality dark-brown hexagonal crystals of **1**·MeCN were collected by filtration, washed with MeCN (2 × 5 mL), and dried under vacuum; the yield was 75%. Anal. Calcd for **1**·MeCN: C, 38.33; H, 3.26; N, 15.10%. Found: C, 38.31; H, 3.10; N, 14.98%. Selected IR data (cm^{-1}): 3334 (m), 3068 (m), 2902 (w), 2784 (m), 2048 (vs), 1602 (s), 1567 (m), 1482 (m), 1434 (s), 1367 (m), 1210 (m), 1291 (m), 1248 (w), 1223 (w), 1153 (m), 1082 (vs), 1048 (m), 1010 (m), 817 (m), 758 (s), 729 (m), 671 (vs), 622 (vs), 549 (m), 467 (m).

$[Mn_{10}O_4(N_3)_4(hmp)_{12}](N_3)_2$ (2). This complex was prepared in the same manner as complex **1** but using $Mn(NO_3)_2\cdot H_2O$ (0.36 g, 2.0 mmol) in place of $Mn(ClO_4)_2\cdot 6H_2O$. After 3 days, dark-brown hexagonal crystals of **2**·MeCN were isolated, collected by filtration, washed with MeCN (2 × 5 mL), and dried under vacuum; the yield was 10%. Anal. Calcd for **2** (solvent-free): C, 39.98; H, 3.36; N, 19.43%. Found: C, 39.77; H, 3.32; N, 19.54%. Selected IR data (cm^{-1}): 3345 (m), 3069 (m), 2905 (w), 2789 (m), 2055 (vs), 1601 (s), 1569 (m), 1481 (m), 1434 (s), 1361 (m), 1210 (m), 1278 (m), 1248 (w), 1222 (w), 1151 (m), 1054 (m), 1011 (m), 820 (m), 757 (s), 733 (m), 614 (vs), 547 (m), 463 (m).

$[Mn_{10}O_2(N_3)_6(pdmH)_4(thme)_4]$ (3). To a stirred solution of $pdmH_2$ (0.28 g, 2.0 mmol), $thmeH_3$ (0.24 g, 2.0 mmol) and Et_3N (0.28 mL, 2.0 mmol) in MeCN/MeOH (20/2 mL) was added solid NaN_3 (0.13 g, 2.0 mmol). The mixture was stirred for a further 30 min and then solid $Mn(ClO_4)_2\cdot 6H_2O$ (0.72 g, 2.0 mmol) was added under vigorous stirring, which caused a rapid color change from pale yellow to dark brown. The solution was stirred for a further 1 h, filtered, and the filtrate was layered with Et_2O (50 mL). After six days, brown crystals of **3**·$2H_2O$·8MeCN appeared and were collected by filtration, washed with MeCN (2 × 5 mL) and Et_2O (2 × 5 mL), and dried under vacuum; the yield was 60%. Anal. Calcd for **3** (solvent-free): C, 31.09; H, 3.70; N, 16.62%. Found: C, 31.38; H, 3.58; N, 16.79%. Selected IR data (cm^{-1}): 3349 (m), 2881 (m), 2067 (vs), 1594 (m), 1451 (m), 1407 (m), 1332 (m), 1286 (w), 1123 (m), 1042 (s), 786 (m), 678 (m), 577 (s).

$[Mn_4(N_3)_4(pdmH)_2(teaH)_2]$ (4). To a stirred solution of $pdmH_2$ (0.28 g, 2.0 mmol), $teaH_3$ (0.30 g, 2.0 mmol), and Et_3N (0.28 mL, 2.0 mmol) in MeCN/MeOH (20/2 mL) was added solid NaN_3 (0.13 g, 2.0 mmol). The mixture was stirred for a further 30 min and then solid $Mn(ClO_4)_2\cdot 6H_2O$ (0.72 g, 2.0 mmol) was added under vigorous stirring, which caused a rapid color change from pale yellow to dark red. The solution was stirred for a further 1 h, filtered, and the filtrate was layered with a mixture of Et_2O and *n*-hexane (50 mL, 1:1 v/v). After four days, red crystals of **4** appeared and were collected by filtration, washed with MeCN (2 × 5 mL) and Et_2O (2 × 5 mL), and dried under vacuum; the yield was 85%. Anal. Calcd for **4**: C, 32.58; H, 4.42; N, 23.38%. Found: C, 32.64; H, 4.38; N, 23.49%. Selected IR data (cm^{-1}): 3184 (mb), 2859 (m), 2074 (vs), 1605 (m), 1579 (m), 1442 (s), 1328 (m), 1285 (m), 1210 (m), 1157 (w), 1097 (m), 1077 (s), 1052 (s), 916 (m), 885 (m), 779 (m), 746 (m), 686 (m), 638 (w), 586 (m), 566 (m), 496 (w), 459 (m).

X-ray Crystallography. Data were collected on a Siemens SMART PLATFORM equipped with a CCD area detector and a graphite monochromator utilizing Mo Kα radiation (λ = 0.71073 Å). Suitable crystals of **1**·MeCN, **2**·MeCN, **3**·$2H_2O$·8MeCN, and **4** were attached to glass fibers using silicone grease and transferred to a goniostat where they were cooled to 173 K for data collection. An initial search for reciprocal space revealed a cubic cell for **1**·MeCN and **2**·MeCN, a monoclinic cell for **3**·$2H_2O$·8MeCN, and a triclinic cell for **4**; the choices of space groups $P4_3/n$ (**1**·MeCN and **2**·MeCN), $P2_1/c$ (**3**·$2H_2O$·8MeCN) and $P\bar{1}$ (**4**) were confirmed by the subsequent solution and refinement of the structures. Cell parameters were refined using up to 8192 reflections. A full sphere of data (1850 frames) was collected using the ω-scan

(24) (a) Foguet-Albiol, D.; O'Brien, T. A.; Wernsdorfer, W.; Moulton, B.; Zaworotko, M. J.; Abboud, K. A.; Christou, G. *Angew. Chem., Int. Ed.* **2005**, *44*, 897. (b) Saalfrank, R. W.; Nakajima, T.; Mooren, N.; Scheurer, A.; Maid, H.; Hampel, F.; Trieflinger, C.; Daub, J. *Eur. J. Inorg. Chem.* **2005**, 1149.

(25) (a) Yoo, J.; Brechin, E. K.; Yamaguchi, A.; Nakano, M.; Huffman, J. C.; Maniero, A. L.; Brunel, L.- C.; Awaga, K.; Ishimoto, H.; Christou, G.; Hendrickson, D. N. *Inorg. Chem.* **2000**, *39*, 3615. (b) Yang, E.- C.; Hendrickson, D. N.; Wernsdorfer, W.; Nakano, M.; Zakharov, L. N.; Sommer, R. D.; Rheingold, A. L.; Ledezma-Gairraud, M.; Christou, G. *J. Appl. Phys.* **2002**, *91*, 7382.

Table 1. Crystallographic Data for **1**·MeCN, **2**·MeCN, **3**·2H_2O·8MeCN, and **4**

Parameter	1	2	3	4
formula[a]	$C_{74}H_{75}Cl_2Mn_{10}N_{25}O_{24}$	$C_{74}H_{75}Mn_{10}N_{31}O_{16}$	$C_{64}H_{96}Mn_{10}N_{30}O_{24}$	$C_{26}H_{42}Mn_4N_{16}O_{10}$
fw, g mol^{-1}[a]	2283.44	2163.00	2219.05	958.52
crystal system	cubic	cubic	monoclinic	triclinic
space group	$P4_3/n$	$P4_3/n$	$P2_1/c$	$P\bar{1}$
a, Å	16.5474(5)	16.3101(3)	14.202(4)	8.7034(6)
b, Å	16.5474(5)	16.3101(3)	12.894(4)	10.5600(7)
c, Å	16.5474(5)	16.3101(3)	21.937(6)	11.4031(8)
α, deg	90	90	90	110.043(1)
β, deg	90	90	102.575(4)	96.032(1)
γ, deg	90	90	90	104.989(1)
V, Å^3	4531.0(2)	4338.80(14)	3920.7(19)	929.14(11)
Z	2	2	2	1
T, K	173(2)	173(2)	173(2)	173(2)
radiation, Å[b]	0.71073	0.71073	0.71073	0.71073
ρ_{calc}, g cm^{-3}	1.674	1.656	1.802	1.713
μ, mm^{-1}	1.459	1.483	1.649	1.404
R1[c,d]	0.0351	0.0266	0.0877	0.0280
wR2[e]	0.0840	0.0577	0.2152	0.0730

[a] Including solvate molecules. [b] Graphite monochromator. [c] $I > 2\sigma(I)$. [d] $R1 = \sum(||F_o| - |F_c||)/\sum|F_o|$. [e] $wR2 = [\sum[w(F_o^2 - F_c^2)^2]/\sum[w(F_o^2)^2]]^{1/2}$, $w = 1/[\sigma^2(F_o^2) + [(ap)^2 + bp]$, where $p = [\max(F_o^2, 0) + 2F_c^2]/3$.

method (0.3° frame width). The first 50 frames were remeasured at the end of data collection to monitor instrument and crystal stability (maximum correction on I was <1%). Absorption corrections by integration were applied based on measured indexed crystal faces. The structures were solved by direct methods in *SHELXTL6*,[26] and refined on F^2 using full-matrix least-squares. The non-H atoms were treated anisotropically, whereas the H atoms were placed in calculated, ideal positions and refined as riding on their respective C atoms. Unit cell parameters and structure solution and refinement data are listed in Table 1.

For **1**·MeCN, the asymmetric unit consists of half-the Mn_{10} cluster and half the ClO_4^- and MeCN. The latter solvent molecule was disordered and could not be modeled properly; thus, program SQUEEZE,[27] a part of the PLATON package of crystallographic software, was used to calculate the solvent disorder area and remove its contribution to the overall intensity data. A total of 107 parameters were included in the structure refinement using 1755 reflections with $I > 2\sigma(I)$ to yield R1 and wR2 of 3.51 and 8.40%, respectively.

For **2**·MeCN, the asymmetric unit consists of half the Mn_{10} cluster (located on a 23 center) and one-eighth of a combination of N_3^- and MeCN disordered in the same position (222 symmetry center). The N_3^- anion and MeCN solvent disorder is the only possibility of balancing the crystal charges where the ratio of cluster-to-anion is 3:1 necessitating 2/3 occupancy of the N_3^- with 1/3 MeCN disorder. A total of 104 parameters were included in the structure refinement using 1670 reflections with $I > 2\sigma(I)$ to yield R1 and wR2 of 2.66 and 5.77%, respectively.

For **3**·2H_2O·8MeCN, the asymmetric unit consists of half the Mn_{10} cluster, and one H_2O and four MeCN molecules of crystallization. The solvent molecules were disordered and could not be modeled properly; thus, the program SQUEEZE was used to calculate the solvent disorder area and remove its contribution to the overall intensity data. A total of 452 parameters were included in the structure refinement on F^2 using 5132 reflections with $I > 2\sigma(I)$ to yield R1 and wR2 of 8.77 and 21.52%, respectively.

For **4**, the asymmetric unit consists of half the Mn_4 cluster. A total of 261 parameters were included in the structure refinement on F^2 using 3379 reflections with $I > 2\sigma(I)$ to yield R1 and wR2 of 2.80 and 7.30%, respectively.

Physical Measurements

Infrared spectra were recorded in the solid state (KBr pellets) on a Nicolet Nexus 670 FTIR spectrometer in the 4000–450 cm^{-1} range. Elemental analyses (C, H, and N) were performed on a Perkin-Elmer 2400 Series II Analyzer. Variable-temperature dc and ac magnetic susceptibility data were collected at the University of Florida using a Quantum Design MPMS-XL SQUID susceptometer equipped with a 7 T magnet and operating in the 1.8–300 K range. Samples were embedded in solid eicosane to prevent torquing. Alternating current magnetic susceptibility measurements were performed in an oscillating ac field of 3.5 G and a zero dc field. The oscillation frequencies were in the 5–1488 Hz range. Magnetization vs field and temperature data were fit using the program MAGNET.[28] Pascal's constants were used to estimate the diamagnetic corrections, which were subtracted from the experimental susceptibilities to give the molar paramagnetic susceptibilities (χ_M). Low-temperature (<1.8 K) hysteresis studies and dc relaxation measurements were performed at Grenoble using an array of micro-SQUIDS.[29] The high sensitivity of this magnetometer allows the study of single crystals of SMMs of the order of 10–500 μm. The field can be applied in any direction by separately driving three orthogonal coils. Crystals were maintained in mother liquor to avoid degradation and were covered in grease for protection during the transfer to the micro-SQUID and subsequent cooling.

Theoretical Calculations

The exchange constants in complex **1** were estimated with the ZILSH method[30] and density functional theory (DFT) calculations. For the ZILSH calculations, unrestricted Hartree–Fock molecular orbital wave functions were obtained

(26) *SHELXTL6*; Bruker-AXS,: Madison, WI, 2000.
(27) Van der Sluis, P.; Spek, A. L. *Acta Crystallogr., Sect. A: Found. Crystallogr.* **1990**, *A46*, 194.
(28) Davidson, E. R. *MAGNET*; Indiana University: Bloomington, IN, 1999.
(29) Wernsdorfer, W. *Adv. Chem. Phys.* **2001**, *118*, 99.
(30) O'Brien, T. A.; Davidson, E. R. *Int. J. Quantum Chem.* **2003**, *92*, 294.

with the INDO/S method of Zerner[31] for various spin components of the complex. These wave functions were assumed to follow an effective Heisenberg spin Hamiltonian given in eq 1, where A and B label

$$\hat{H}_{\text{eff}} = \hat{H}_0 - 2\sum_{A<B} J_{AB}\,\hat{S}_A \cdot \hat{S}_B \qquad (1)$$

metal centers and $\hat{H}_0$ contains all spin-independent terms in the electronic Hamiltonian. The expectation value of $\hat{H}_{\text{eff}}$ for a spin component wave function Ψ_i is given in eq 2, where E_0

$$E^{\text{UHF},i} = E_0 - 2\sum_{A<B} J_{AB}\langle \hat{S}_A \cdot \hat{S}_B\rangle^{\text{UHF},i} \qquad (2)$$

contains all spin-independent contributions to the energy. Spin couplings $\langle \hat{S}_A \cdot \hat{S}_B\rangle^{\text{UHF}}$ were calculated with the semiempirical local spin operator of Davidson and O'Brien.[30,32] Given energies and spin couplings for the appropriate number of spin components (forty six for **1**), eqs 2 were solved simultaneously for the parameters E_0 and J_{AB} for all unique combinations of A and B. The spin components used were the ones with all unpaired spins aligned parallel, and the forty five components with unpaired spins on all unique combinations of two metal ions reversed.

A similar strategy was used in the DFT calculations by assuming that energies of unrestricted Kohn–Sham determinants representing the spin components also follow eqs 2. Following our standard procedure, ZILSH spin couplings were used with DFT energies to obtain estimates of the exchange constants. Spin couplings computed with the ZILSH method are generally similar to those obtained from DFT densities.[30,32,33] The B3LYP functional[34] was used for all DFT calculations, which were performed with the Gaussian03 program.[35] Two basis sets were employed, either the triple-ζ TZVP basis set of Alrichs[36] for Mn atoms and the double-ζ DZVP basis set of Alrichs[37] for lighter atoms (basis set I), or the triple-ζ TZVP basis set of Alrichs[36] on all atoms (basis set II). Owing to the large size of the complex, DFT calculations were applied to a smaller model cluster to refine certain exchange constants obtained from ZILSH calculations on the full complex (vide infra). We have used a similar approach previously,[24a] as have others.[18b,38]

An important quantity obtained from both ZILSH and DFT calculations was the local spin density for each metal atom, equal to the number of unpaired electrons (N_i) on metal atom "*i*".[30] The signs of the N_i indicate the spin alignments within the complex for a particular spin component. The local spin densities were used to check that the correct spin component wave functions (or densities, in the case of DFT calculations) were obtained from the calculations (vide infra).

Once the exchange constants (J_{AB}) were obtained, wave functions and energies of the spin eigenstates described by the Heisenberg spin model could be obtained by substituting the J_{AB} into the Heisenberg spin Hamiltonian (eq 1 with $\hat{H}_0 = 0$) and diagonalizing the operator in the basis of spin components $\varphi_i = |M_1\ M_2\ \cdots\ M_N\rangle_i$, where M_A is the formal local *z* component of spin of metal "A" (i.e., $M_A = {}^5/_2$ for high spin d^5 Mn^{II} ions, $M_A = 2$ for high spin d^4 Mn^{III} ions). The wave functions of the spin eigenstates are then linear combinations of the basis functions ϕ_i,

$$|\psi_S\rangle^I = \sum_i C_i\varphi_i = \sum_i C_i|M_1\ M_2\ \cdots\ M_N\rangle_i \qquad (3)$$

as given by eq 3. In the case of a ground-state with nonzero spin, the component making the leading contribution to the wave function (i.e., that with the largest weighting coefficient C_i) indicates the spin alignments in the ground state. Complex **1** is too large to be treated with full matrix diagonalization, so the more efficient Davidson algorithm[39] was used to extract the energy and wave function for the lowest energy state of each spin.

Results and Discussion

Syntheses. Many synthetic procedures to polynuclear manganese clusters rely on the reaction of triangular $[Mn_3O(O_2CR)_6L_3]^+$ species with a potentially chelating ligand. In particular, pyridyl alcohols, such as hmpH, the related 2-(hydroxyethyl)pyridine (hepH), and $pdmH_2$ have given products such as $[Mn_{10}O_4(OH)_2(O_2CMe)_8(hmp)_8]^{4+}$,[20a] $[Mn_{18}O_{14}(O_2CMe)_{18}(hep)_4(hepH)_2(H_2O)_2]^{2+}$,[40] and $[Mn_4$-

(31) (a) Zerner, M. C.; Loew, G. H.; Kirchner, R. F.; Muellerwesterhoff, U. T. *J. Am. Chem. Soc.* **1980**, *102*, 589. (b) Ridley, J. E.; Zerner, M. C. *Theor. Chim. Acta* **1973**, *32*, 111. (c) Kotzian, M.; Rosch, N.; Zerner, M. C. *Theor. Chim. Acta* **1992**, *81*, 201. (d) Culberson, J. C.; Knappe, P.; Rosch, N.; Zerner, M. C. *Theor. Chim. Acta* **1987**, *71*, 21. (e) Cory, M. G.; Kostlmeier, S.; Kotzian, M.; Rosch, N.; Zerner, M. C. *J. Chem. Phys.* **1994**, *100*, 1353. (f) Bacon, A. D.; Zerner, M. C. *Theor. Chim. Acta* **1979**, *53*, 21. (g) Anderson, W. P.; Cundari, T. R.; Zerner, M. C. *Int. J. Quantum Chem.* **1991**, *39*, 31. (h) Anderson, W. P.; Cundari, T. R.; Drago, R. S.; Zerner, M. C. *Inorg. Chem.* **1990**, *29*, 1.

(32) (a) Davidson, E. R.; Clark, A. E. *Mol. Phys.* **2002**, *100*, 373. (b) Clark, A. E.; Davidson, E. R. *J. Chem. Phys.* **2001**, *115*, 7382.

(33) Davidson, E. R.; Clark, A. E. *J. Phys. Chem. A* **2002**, *106*, 7456.

(34) (a) Lee, C.; Yang, W.; Parr, R. G. *Phys. Rev. B* **1988**, *37*, 785. (b) Becke, A. D. *J. Chem. Phys.* **1993**, *98*, 5648.

(35) Frisch, M. J.; Trucks, G. W.; Schlegel, H. B.; Scuseria, G. E.; Robb, M. A.; Cheeseman, J. R.; Montgomery, J. A., Jr.; Vreven, T.; Kudin, K. N.; Burant, J. C.; Millam, J. M.; Iyengar, S. S.; Tomasi, J.; Barone, V.; Mennucci, B.; Cossi, M.; Scalmani, G.; Rega, N.; Petersson, G. A.; Nakatsuji, H.; Hada, M.; Ehara, M.; Toyota, K.; Fukuda, R.; Hasegawa, J.; Ishida, M.; Nakajima, T.; Honda, Y.; Kitao, O.; Nakai, H.; Klene, M.; Li, X.; Knox, J. E.; Hratchian, H. P.; Cross, J. B.; Adamo, C.; Jaramillo, J.; Gomperts, R.; Stratman, R. E.; Yazyev, O.; Austin, A. J.; Cammi, R.; Pomell, C.; Ochterski, J. W.; Ayala, P. Y.; Morokuma, K.; Voth, G. A.; Salvador, P.; Dannenberg, J. J.; Zakrzewski, V. G.; Dapprich, S.; Daniels, A. D.; Strain, M. C.; Farkas, O.; Malick, D. K.; Rabuck, A. D.; Raghavachari, K.; Foresman, J. B.; Ortiz, J. V.; Cui, Q.; Baboul, A. G.; Clifford, S.; Cioslowski, J.; Stefanov, B. B.; Liu, G.; Liashenko, A.; Piskorz, P.; Komaromi, I.; Martin, R. L.; Fox, D. J.; Keith, T.; Al-Laham, M. A.; Peng, C. Y.; Nanayakkara, A.; Challacombe, M.; Gill, P. M. W.; Johnson, B.; Chen, W.; Wong, M. W.; Gonzalez, C.; Pople, J. A. *Gaussian03*, Revision B.05; Gaussian, Inc.: Pittsburgh, PA, 2003.

(36) Schaefer, A.; Horn, H.; Ahlrichs, R. *J. Chem. Phys.* **1994**, *100*, 5829.

(37) Schaefer, A.; Horn, H.; Ahlrichs, R. *J. Chem. Phys.* **1992**, *97*, 2571.

(38) (a) Cano, J.; Alemany, P.; Alvarez, S.; Verdaguer, M.; Ruiz, E. *Chem.—Eur. J.* **1998**, *4*, 476. (b) Ruiz, E.; Cano, J.; Alvarez, S.; Alemany, P. *J. Comput. Chem.* **1999**, *20*, 1391. (c) Ruiz, E.; Rodriguez-Fortea, A.; Cano, J.; Alvarez, S. *J. Comput. Chem.* **2003**, *24*, 982. (d) Carrasco, R.; Cano, J.; Mallah, T.; Jones, L. F.; Collison, D.; Brechin, E. K. *Inorg. Chem.* **2004**, *43*, 5410.

(39) Davidson, E. R. *J. Comput. Phys.* **1975**, *17*, 87.

(40) Brechin, E. K.; Sanudo, E. C.; Wernsdorfer, W.; Boskovic, C.; Yoo, J.; Hendrickson, D. N.; Yamaguchi, A.; Ishimoto, H.; Concolino, T. E.; Rheingold, A. L.; Christou, G. *Inorg. Chem.* **2005**, *44*, 502.

$(O_2CMe)_2(pdmH)_6]^{2+}$,[25a] whereas tripodal ligands, such as $thmeH_3$, have led to a large family of rod-like manganese carboxylate clusters,[41] among others.[22] As stated earlier, the present study explored reactions involving such chelates and azide groups, as well as avoiding the presence of carboxylate groups.[8,15,42]

A variety of reactions differing in the azide amount, the Mn/hmpH/NEt_3 ratio, and/or the solvent were explored in identifying the following successful systems. The reaction of $Mn(ClO_4)_2 \cdot 6H_2O$ or $Mn(NO_3)_2 \cdot H_2O$, hmpH, NEt_3 and NaN_3 in a 1:1:1:1 ratio in MeCN/MeOH gave the decanuclear complex $[Mn_{10}O_4(N_3)_4(hmp)_{12}]X_2$ ($X = ClO_4^-$ (**1**), N_3^- (**2**)) in high (~75%) and low (~10%) yields, respectively. The formation of the cation is summarized in eq 4. The

$$10Mn^{2+} + 12hmpH + 14NEt_3 + 4N_3^- + \frac{3}{2}O_2 + H_2O \rightarrow [Mn_{10}O_4(N_3)_4(hmp)_{12}]^{2+} + 14NHEt_3^+ \quad (4)$$

reaction is an oxidation, undoubtedly by O_2 under the prevailing basic conditions, and has been balanced accordingly. The NEt_3 has the role of proton acceptor to facilitate both the deprotonation of the hmpH groups and H_2O molecules as a source of additional O^{2-} ions. In the absence of NEt_3, pale yellow solutions were obtained, indicative of Mn^{II} species. On the other hand, greater than one equiv of NEt_3 rapidly gave insoluble amorphous precipitates that were probably polymeric. Increase in the amount of hmpH to 2 equiv (or more) did not give **1** or **2**, but instead the tetranuclear, mixed-valence ($2Mn^{II}$, $2Mn^{III}$) products, $[Mn_4(N_3)_4(hmp)_6]$[42b] and $[Mn_4(NO_3)_4(hmp)_6]$,[20b] respectively, in good yields (>40%).

As often seen in transition metal cluster chemistry,[22,43] the reaction products are solvent dependent. Using only MeCN as the solvent gave $[Mn_4(N_3)_4(hmp)_6]$[42b] with terminal azides as the only isolable product in 15% yield, but contaminated with uncharacterized solid products. Similarly, using only MeOH as solvent gave known $[Mn^{II}_2Mn^{III}_2(N_3)_2(hmp)_6]_n^{2+}$,[20d] which is a one-dimensional chain with bridging μ-1,3-azido groups. Nonpolar solvents such as CH_2Cl_2 and $CHCl_3$ required much longer reaction times and only gave similar azide-free Mn_4 products in very low yields (<10%). It is clear that these reaction systems are very complicated, undoubtedly with many species in equilibrium, and thus are sensitive to small changes in the reaction conditions.

A number of Mn/N_3^- reactions with $pdmH_2$ in MeCN/MeOH were also investigated, but the only isolable product was known $[Mn_{25}O_{18}(OH)_2(N_3)_{12}(pdm)_6(pdmH)_6]^{2+}$.[8] We thus further explored mixed-chelate reaction systems, such as had recently yielded the new $[Mn_{25}O_{18}(OH)(OMe)(hmp)_6(pdm)_6(pdmH)_6]^{8+}$ complex with hmpH and $pdmH_2$,[9] and chose the $pdmH_2$/$thmeH_3$ and $pdmH_2$/$teaH_3$ combinations. The reaction of $Mn(ClO_4)_2 \cdot 6H_2O$, $pdmH_2$, $thmeH_3$, NaN_3, and NEt_3 in a 1:1:1:1:1 ratio in MeCN/MeOH gave the decanuclear complex $[Mn_{10}O_2(N_3)_6(pdmH)_4(thme)_4]$ (**3**) in ~60% yield (eq 5).

$$10Mn^{2+} + 4pdmH_2 + 4thmeH_3 + 14NEt_3 + 6N_3^- + \frac{3}{2}O_2 \rightarrow [Mn_{10}O_2(N_3)_6(pdmH)_4(thme)_4] + 14NHEt_3^+ + H_2O \quad (5)$$

The same reaction but with $teaH_3$ instead of $thmeH_3$ gave instead the tetranuclear complex $[Mn_4(N_3)_4(pdmH)_2(teaH)_2]$ (**4**) in ~85% yield (eq 6).

$$4Mn^{2+} + 2pdmH_2 + 2teaH_3 + 6NEt_3 + 4N_3^- + \frac{3}{2}O_2 \rightarrow [Mn_4(N_3)_4(pdmH)_2(teaH)_2] + 6NHEt_3^+ + 3H_2O \quad (6)$$

Reactions in MeCN with larger $pdmH_2$/Mn/$thmeH_3$ and/or $pdmH_2$/Mn/$teaH_3$ ratios of 2:1:1 or 3:1:1 gave only $[Mn_4(N_3)_4(pdmH)_6]$[42b] and uncharacterized powders, whereas the 1:1:2 or 1:1:3 ratios gave powders we have not been able to crystallize for characterization. Similar reactions in MeOH gave only yellow solutions indicative of Mn^{II} species. In contrast, small changes to the amount of NEt_3 had no effect on the product complexes **3** and **4**, as long as the mixed MeCN/MeOH solvent system was retained.

Description of Structures. The partially labeled structure and stereoview of the cation of complex **1** are shown in Figure 1. Selected interatomic distances and angles are listed in Table 2. Complexes **1** and **2** crystallize in the high symmetry cubic space group $P4_3/n$; complex **2** contains the same cation as **1**, and it will not be further discussed. The structure of the $[Mn_{10}O_4(N_3)_4(hmp)_{12}]^{2+}$ cation consists of ten Mn ions with a tetra-face-capped octahedral topology. The central octahedron of six Mn^{III} atoms (Mn2) is bridged on each face by four μ_3-N_3^- and four μ_4-O^{2-} ions (Figure 2, top), with the latter (O1) also bridging to four extrinsic Mn^{II} atoms (Mn1) that thus form a Mn^{II}_4 tetrahedron above four nonadjacent faces of the octahedron. The μ_4-O^{2-} atom O1 has a distinctly trigonal pyramidal geometry with $Mn^{III}-O-Mn^{III}$ and $Mn^{II}-O-Mn^{III}$ angles of 116.3(8) and 101.2(1)°, respectively. The μ_3-N_3^- ions bind in a μ_3-1,1,1 (end-on) fashion first seen bridging paramagnetic ions in the $[Ni_4(\mu_3\text{-}N_3)_4]^{4+}$ cubic core.[44] The peripheral ligation in **1** is provided by twelve hmp^- groups; three of these chelate each Mn^{II} atom and bridge with their alkoxide arms to different Mn^{III} atoms. The $[Mn_{10}(\mu_4\text{-}O)_4(\mu_3\text{-}N_3)_4]^{14+}$ core has T_d symmetry (Figure 2, bottom), but inclusion of the hmp^- groups removes the σ_d planes and S_4 axes, and the complete cation consequently has rare T point group symmetry, which is crystallographically imposed; point group T is the rotational subgroup of T_d. This aesthetically pleasing symmetry extends, of course, to the packing of molecules in the crystal; a packing diagram is available in Supporting Information.

(41) Rajaraman, G.; Murugesu, M.; Sanudo, E. C.; Soler, M.; Wernsdorfer, W.; Helliwell, M.; Muryn, C.; Raftery, J.; Teat, S. J.; Christou, G.; Brechin, E. K. *J. Am.Chem. Soc.* **2004**, *126*, 15445.

(42) (a) Stamatatos, Th. C.; Luisi, B. S.; Moulton, B.; Christou, G. *Inorg. Chem.* **2008**, *47*, 1134. (b) Stamatatos, Th. C.; Abboud, K. A.; Wernsdorfer, W.; Christou, G., to be submitted.

(43) Brockman, J. T.; Stamatatos, Th. C.; Wernsdorfer, W.; Abboud, K. A.; Christou, G. *Inorg. Chem.* **2007**, *46*, 9160.

(44) (a) Halcrow, M. A.; Huffman, J. C.; Sun, S.- J.; Christou, G. *Angew. Chem., Int. Ed. Engl.* **1995**, *34*, 889. (b) Halcrow, M. A.; Sun, S.- J.; Huffman, J. C.; Christou, G. *Inorg. Chem.* **1995**, *34*, 4167.

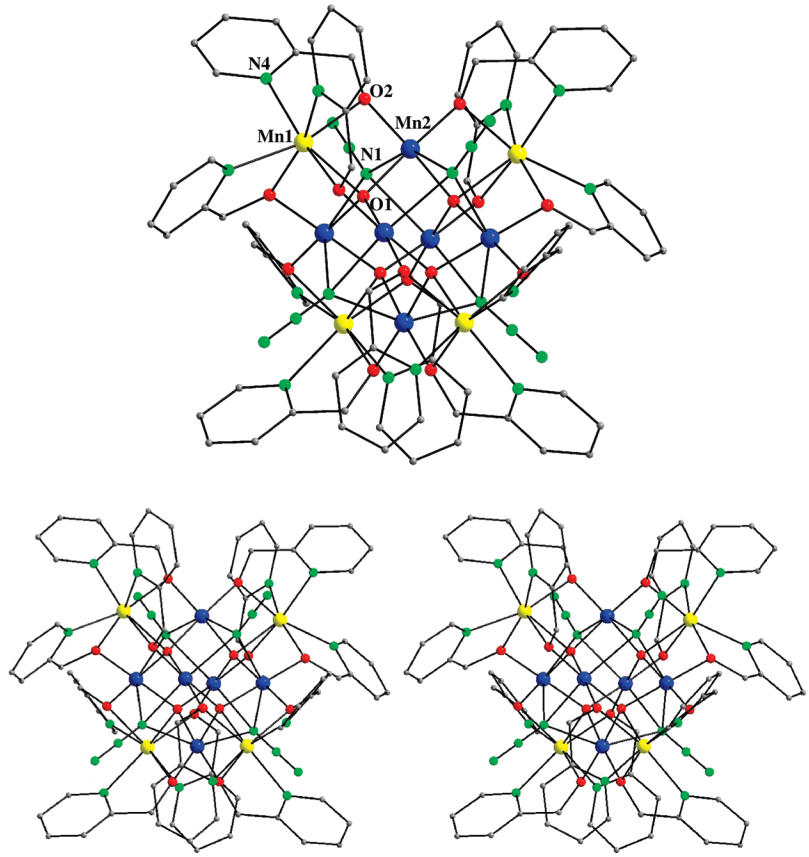

Figure 1. Labeled PovRay representation (top) and stereopair (bottom) of complex **1**, with H atoms omitted for clarity. Color scheme: Mn^{II}, yellow; Mn^{III}, blue; O, red; N, green; C, gray.

Table 2. Selected Interatomic Distances (Å) and Angles (deg) for **1**·MeCN[a]

parameter		parameter	
Mn(1)···Mn(2)	3.267(1)	Mn(1)···Mn(1′)	6.534(1)
Mn(1)−O(1)	2.308(5)	Mn(2)···Mn(2′)	3.239(1)
Mn(1)−O(2)	2.233(3)	Mn(1)−N(4)	2.294(3)
Mn(1)−O(2′)	2.233(3)	Mn(1)−N(4′)	2.294(3)
Mn(1)−O(2″)	2.233(3)	Mn(1)−N(4″)	2.294(3)
Mn(2)−O(1)	1.907(1)	Mn(2)−O(2′)	1.889(3)
Mn(2)−O(1′)	1.907(1)	Mn(2)−N(1)	2.415(4)
Mn(2)−O(2)	1.889(3)	Mn(2)−N(1′)	2.415(4)
Mn(1)−O(1)−Mn(2)	101.2(1)	Mn(2)−O(1)−Mn(2′)	116.3(8)
Mn(1)−O(2)−Mn(2)	104.5(1)	Mn(2)−N(1)−Mn(2′)	84.2(1)

[a] Unprimed, primed, and double-primed atoms are related by symmetry.

Mn^{III} atom Mn2 is six-coordinate with distorted octahedral geometry, whereas Mn^{II} atom Mn1 is seven-coordinate with distorted face-capped octahedral geometry, the capping atom being the oxide atom O1 ($Mn1\text{-}O^{2-}$ = 2.308(5) Å). The Mn oxidation states were obvious from the metric parameters and were confirmed by bond valence sum (BVS)[45] calculations (Table 3). The BVS calculations also confirm that the hmp^- is indeed deprotonated, as expected from its bridging mode. The six Mn^{III} atoms show the Jahn–Teller (JT) distortion expected for a high-spin d^4 ion in near-octahedral geometry, taking the form of an axial elongation of the two trans $Mn-N_{az}$ bonds (2.415(4) Å). Thus, as is almost always the case, the JT elongation axes avoid the $Mn^{III}-O^{2-}$ bonds, the shortest and strongest in the cation.[46] Neither complex **1** nor complex **2** form any significant intermolecular hydrogen-bonds, only weak intermolecular contacts between C−H bonds and the π-system of hmp^- groups.

Triply bridging, end-on N_3^- ions have been observed before in Mn chemistry only in $[Mn_4O_3(N_3)(O_2CR)_3(dbm)_3]$[47] ($dbm^-$ is the anion of dibenzoylmethane), in which the μ_3-1,1,1 N_3^- is at the vertex of a distorted cubane, and in the recently reported $[Mn_{19}O_8(N_3)_8(HL)_{12}(MeCN)_6]^{2+}$ (H_3L = 2,6-bis(hydroxymethyl)-4-methylphenol),[10] in which two μ_3-1,1,1 N_3^- groups bridge faces of a Mn^{III}_6 octahedron. In each molecule, the μ_3-N_3^- lies on a JT axially elongated site with Mn−N lengths in the 2.30–2.36 Å range, slightly less than in **1** and **2** (Mn−N = 2.41 Å).

The partially labeled structure and stereoview of complex **3** is shown in Figure 3, and selected interatomic distances and angles are listed in Table 4. Complex **3** crystallizes in the monoclinic space group $P2_1/c$ and possesses crystallographic C_i symmetry. The core consists of ten Mn ions arranged as two edge-fused octahedra (Figure 4, top), each with a central μ_4-O^{2-} ion (O1, O1′). Charge considerations and the metric parameters indicate the same $Mn^{III}_6Mn^{II}_4$ mixed-valence situation as **1**/**2**, as confirmed by BVS

(45) (a) Brown, I. D.; Altermatt, D. *Acta Crystallogr.* **1985**, *B41*, 244. (b) Liu, W.; Thorp, H. H. *Inorg. Chem.* **1993**, *32*, 4102.

(46) Chakov, N. E.; Lee, S.-C.; Harter, A. G.; Kuhns, P. L.; Reyes, A. P.; Hill, S. O.; Dalal, N. S.; Wernsdorfer, W.; Abboud, K. A.; Christou, G. *J. Am. Chem. Soc.* **2006**, *128*, 6975.

(47) Wemple, M. W.; Adams, D. M.; Hagen, K. S.; Folting, K.; Hendrickson, D. N.; Christou, G. *J. Chem. Soc., Chem. Commun.* **1995**, 1591.

(48) Canada-Vilalta, C.; Pink, M.; Christou, G. *Dalton Trans.* **2003**, 1121.

(49) Papatriantafyllopoulou, C.; Raptopoulou, C. P.; Escuer, A.; Milios, C. J. *Inorg. Chim. Acta* **2007**, *360*, 61.

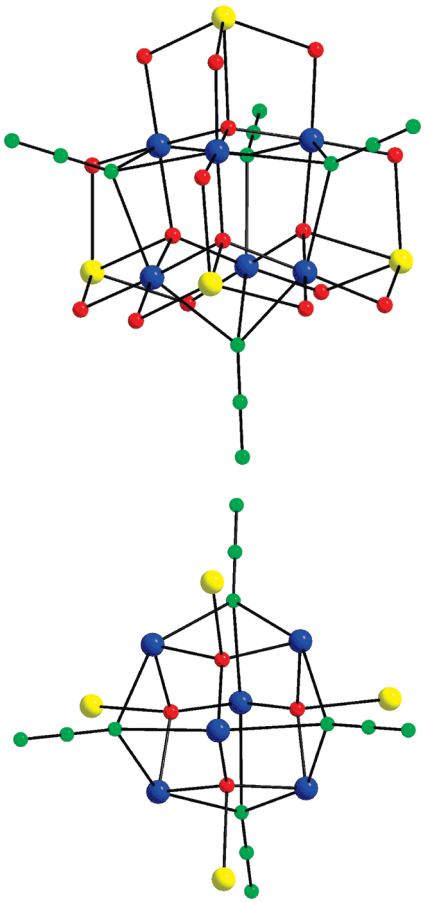

Figure 2. (top) PovRay representation of the complete $[Mn_{10}(\mu_4\text{-}O)_4(\mu_3\text{-}N_3)_4(\mu\text{-}OR)_{12}]^{2+}$ core of **1**; the hmp^- ligands, except for their O atoms, have been omitted. (bottom) The central $[Mn_{10}(\mu_4\text{-}O)_4(\mu_3\text{-}N_3)_4]^{14+}$ core. Color scheme: Mn^{II}, yellow; Mn^{III}, blue; O, red; N, green.

calculations (Table 5), which identified Mn1 and Mn2 as the Mn^{II} atoms and the others as Mn^{III}. The latter was consistent with the Jahn–Teller (JT) axial elongations at Mn3, Mn4, and Mn5. All Mn atoms are six-coordinate with distorted octahedral geometry. The protonation levels of the O atoms were also confirmed by BVS calculations (Table 5). Four $Mn-\mu_4\text{-}O^{2-}-Mn$ angles range from 83.8(2) to 96.6(3)°, whereas the fifth one (Mn3−O1−Mn5) is 172.8(4)°, deviating slightly from the 86.8/101.5° and 180.0° ideal values, respectively, of a very rare seesaw-geometry for oxide atom O1. However, two additional, longer separations, Mn1···O1 (2.811 Å) and Mn2···O1 (2.678 Å) suggest that the true coordination number of O1 is six, with very distorted octahedral geometry. That this is the case is supported by the BVS of O1, which only approaches the value of two

Table 3. Bond Valence Sum (BVS)[a,b] Calculations for Mn and Oxygen Atoms in **1**

atom	Mn^{II}	Mn^{III}	Mn^{IV}
Mn1	1.778	1.674	1.680
Mn2	3.226	2.974	3.085
	BVS	Assignment	Group
O1	1.99	O^{2-}	O^{2-}
O2	1.79	RO^-	hmp^-

[a] The underlined value is the one closest to the charge for which it was calculated. The oxidation state is the nearest whole number to the underlined value. [b] An O BVS in the ∼1.8–2.0, ∼1.0–1.2, and ∼0.2–0.4 ranges is indicative of non-, single- and double-protonation, respectively.

expected for an oxide if all six contacts are included. The Mn atoms are additionally bridged by two $\mu-1,1$ (end-on) N_3^- ions, four RO^- arms of four $pdmH^-$ groups, and twelve RO^- arms of four tripodal $thme^{3-}$ groups. The $pdmH^-$ groups are tridentate-chelating to a Mn^{II} atom, with their deprotonated alkoxide arm bridging to an adjacent Mn^{III} atom; these groups are thus $\eta^1{:}\eta^1{:}\eta^2{:}\mu$ (Figure 5). The four $thme^{3-}$ groups bind with each alkoxide arm bridging either a Mn^{III}_2 or a $Mn^{III}Mn^{II}$ pair of a Mn_3 triangular unit, with one arm also bridging to a third extrinsic Mn^{II} atom. The $thme^{3-}$ groups are thus $\eta^2{:}\eta^2{:}\eta^3{:}\mu_4$ (Figure 5). Peripheral ligation is completed by four terminal azide groups. The complex thus contains a $[Mn_{10}(\mu_4\text{-}O)_2(\mu\text{-}N_3)_2(\mu_3\text{-}OR)_4(\mu\text{-}OR)_{12}]^{4+}$ core (Figure 4, bottom). Finally, the structure contains strong intramolecular OH···N hydrogen-bonds between the $pdmH^-$ OH groups and a terminal azide (O(3)···N(11) = 2.526 Å) and also intermolecular OH···N hydrogen-bonds between a different $pdmH^-$ OH group and a terminal azide in a neighboring molecule (O(5)···N(10) = 2.762 Å).

Complexes **1**−**3** join a small family of known Mn_{10} clusters, and these are collected in Table 6 for convenient comparison. Complex **1** was the first at the $Mn^{II}_4Mn^{III}_6$ oxidation level and has since been joined by $[Mn_{10}O_4Br_4(amp)_6(ampH_2)_3(ampH_3)]^{3+}$,[51] which has the same core as **1** and **2** but with $\mu_3\text{-}Br^-$ rather than $\mu_3\text{-}N_3^-$ groups. The same core is also found in $[Mn_{10}O_4Cl_{12}(biphen)_4]^{4-}$ but at a lower oxidation level of $Mn^{II}_6Mn^{III}_4$ and with $\mu_3\text{-}Cl^-$ instead of $\mu_3\text{-}N_3^-$ groups.[50] It should also be noted that **3** is the first Mn_{10} complex with two types of chelate groups.

The partially labeled structure of complex **4** is shown in Figure 6, and selected interatomic distances and angles are listed in Table 7. The complex lies on an inversion center (space group $P\bar{1}$) and contains a planar Mn_4 rhombus. Each Mn_3 triangular unit is μ_3-bridged by an oxygen atom (O4, O4′) from a tridentate-chelating $teaH^-$ group, whose second alkoxide arm (O3, O3′) is bridging two adjacent Mn atoms (Mn1/Mn2 and Mn1′/Mn2′), whereas its protonated oxygen atom (O5, O5′) is unbound; these groups are thus $\eta^2{:}\eta^1{:}\eta^3{:}\mu_4$ (Figure 5). The $pdmH^-$ groups are also tridentate-chelating to a Mn atom (Mn1, Mn1′), with their deprotonated alkoxide arm (O2, O2′) bridging to an adjacent Mn atom (Mn2′, Mn2); these groups are thus $\eta^1{:}\eta^1{:}\eta^2{:}\mu$ (Figure 5). Four terminal N_3^- groups complete the ligation and make all Mn atoms six-coordinate with distorted octahedral geometries. The complex thus contains a $[Mn_4(\mu_3\text{-}OR)_2(\mu\text{-}OR)_4]^{4+}$ core (Figure 6). Charge considerations and inspection of the metric parameters indicate a $Mn^{III}_2Mn^{II}_2$ mixed-valence situation, as confirmed by BVS calculations that gave values of 2.01 for Mn1 and 2.94 for Mn2. Mn2 also displays a Jahn–Teller

(50) Goldberg, D. P.; Caneschi, A.; Lippard, S. J. *J. Am.Chem. Soc.* **1993**, *115*, 9299.
(51) Manoli, M.; Johnstone, R. D. L.; Parsons, S.; Murrie, M.; Affronte, M.; Evangelisti, M.; Brechin, E. K. *Angew. Chem., Int. Ed.* **2007**, *46*, 4456.
(52) Cavaluzzo, M.; Chen, Q.; Zubieta, J. *J. Chem. Soc., Chem. Commun.* **1993**, 131.
(53) Moushi, E.; Lampropoulos, C.; Wernsdorfer, W.; Nastopoulos, V.; Christou, G.; Tasiopoulos, A. J. *Inorg. Chem.* **2007**, *46*, 3795.
(54) John, R. P.; Lee, K.; Kim, B. J.; Suh, B. J.; Rhee, H.; Lah, M. S. *Inorg. Chem.* **2005**, *44*, 7109.

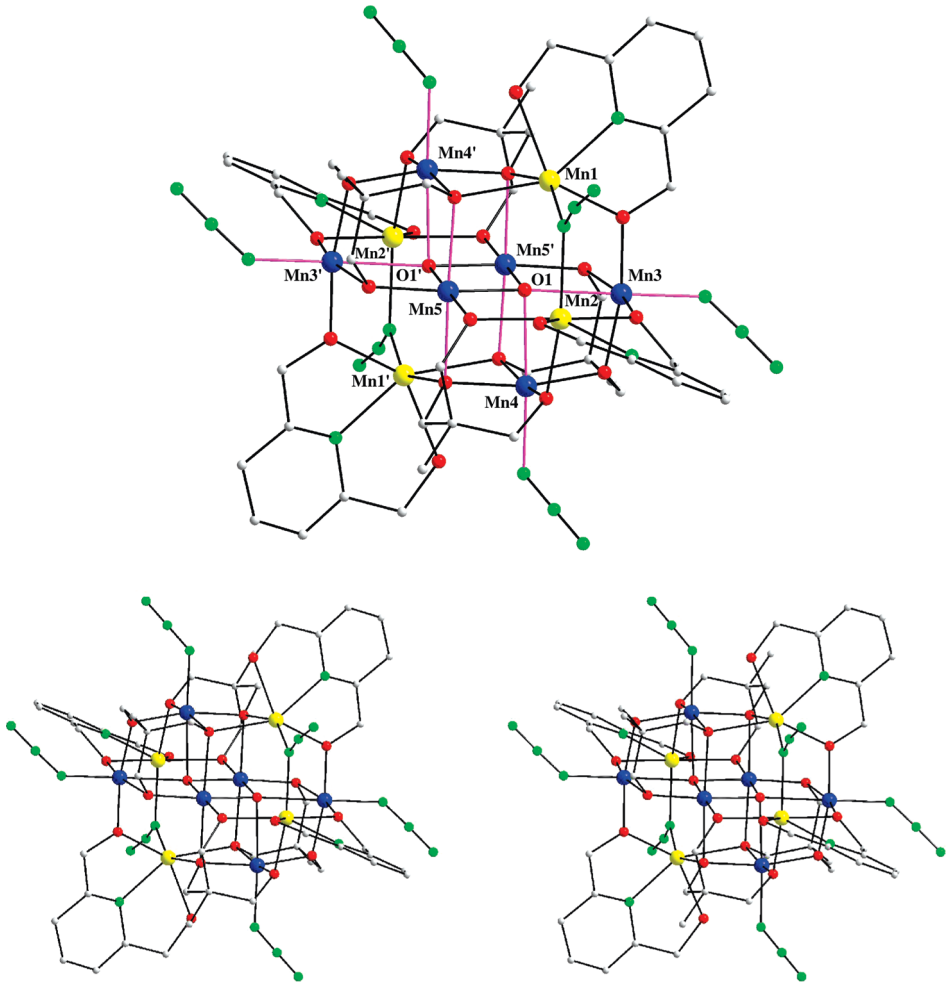

Figure 3. Labeled PovRay representation (top) and stereopair (bottom) of complex **3**, with H atoms omitted for clarity, emphasizing the six Mn^{III} Jahn–Teller axes. Color scheme: Mn^{II}, yellow; Mn^{III}, blue; O, red; N, green; C, gray.

Table 4. Selected Interatomic Distances (Å) and Angles (deg) for **3**·$2H_2O$·8MeCN[a]

Parameter		Parameter	
Mn(1)···Mn(2)	3.624(3)	Mn(2)···Mn(5)	4.579(4)
Mn(1)···Mn(3)	3.515(5)	Mn(3)···Mn(4)	3.142(2)
Mn(1)···Mn(4)	5.104(8)	Mn(3)···Mn(5)	4.300(7)
Mn(1)···Mn(5)	3.571(3)	Mn(3)···Mn(5′)	3.076(9)
Mn(1)···Mn(5′)	3.489(8)	Mn(4)···Mn(5)	3.142(2)
Mn(2)···Mn(3)	3.393(3)	Mn(4)···Mn(5′)	3.180(2)
Mn(2)···Mn(4)	3.447(8)	Mn(5)···Mn(5′)	2.852(3)
Mn(1)−O(2)	2.158(7)	Mn(3)−O(10)	1.958(7)
Mn(1)−O(3)	2.315(2)	Mn(3)−O(11)	1.959(7)
Mn(1)−O(8′)	2.168(7)	Mn(3)−N(8)	2.130(1)
Mn(1)−O(9′)	2.302(9)	Mn(4)−O(1)	2.335(7)
Mn(1)−N(1)	2.213(3)	Mn(4)−O(7)	1.856(7)
Mn(1)−N(5)	2.142(9)	Mn(4)−O(8)	1.972(8)
Mn(2)−O(4)	2.190(8)	Mn(4)−O(9)	1.960(7)
Mn(2)−O(5)	2.325(9)	Mn(4)−O(11)	1.968(8)
Mn(2)−O(6)	2.147(8)	Mn(4)−N(11)	2.163(1)
Mn(2)−O(7)	2.245(8)	Mn(5)−O(1)	1.940(8)
Mn(2)−N(2)	2.250(9)	Mn(5)-O(1′)	1.906(7)
Mn(2)−N(5)	2.223(1)	Mn(5)−O(6)	1.903(7)
Mn(3)−O(1)	2.368(8)	Mn(5)−O(8)	2.282(8)
Mn(3)−O(2)	1.904(7)	Mn(5)−O(9′)	2.289(7)
Mn(3)−O(4)	1.883(7)	Mn(5)−O(10′)	1.945(8)
Mn(3)−O(1)−Mn(4)	83.8(2)	Mn(3)−O(1)−Mn(5′)	91.4(3)
Mn(3)−O(1)−Mn(5)	172.8(4)	Mn(4)−O(1)−Mn(5)	94.1(3)
Mn(4)−O(1)−Mn(5′)	96.6(3)	Mn(5)−O(1)−Mn(5′)	95.7(3)

[a] Primed and unprimed atoms are related by symmetry.

(JT) distortion as expected for high-spin d^4 ion in near-octahedral geometry, taking the form of an elongation of the O4′−Mn2−N8 and symmetry-related O4−Mn2′−N8′ axes. Thus, Mn2−O4′ [2.240(1) Å] and Mn2−N8 [2.382(2) Å] are distinctly longer than the other four bond lengths [1.902(1)−1.975(2) Å].

Finally, the structure contains intermolecular OH···O hydrogen-bonds between the $pdmH^-$ OH groups and $teaH^-$ groups in a neighboring molecule (O(1)···O(5) = 2.653 Å), as well as intermolecular OH···N hydrogen-bonds between a $teaH^-$ OH group and a terminal azide in a neighboring molecule (O(5)···N(1) = 2.764 Å). These interactions serve to link neighboring Mn_4 molecules in the crystal into two-dimensional sheets in the crystallographic *bc* plane (see Supporting Information).

There have been a large number of Mn_4 complexes reported in the literature, and these possess a wide variety of metal topologies such as linear units, rectangles, rhombs, cubanes, butterflies, and so forth. The $[Mn_4(\mu_3\text{-}OR)_2(\mu\text{-}OR)_4]^{4+}$ core of **4** has already been found in a few $Mn^{III}_2Mn^{II}_2$ compounds with alkoxide-based ligands;[20b,d,21b,24a,25a,59] however, **4** is the first such example with two different types of alkoxide-containing chelates.

Magnetochemistry

Magnetic Susceptibility Studies. Variable-temperature, solid state magnetic susceptibility measurements were per-

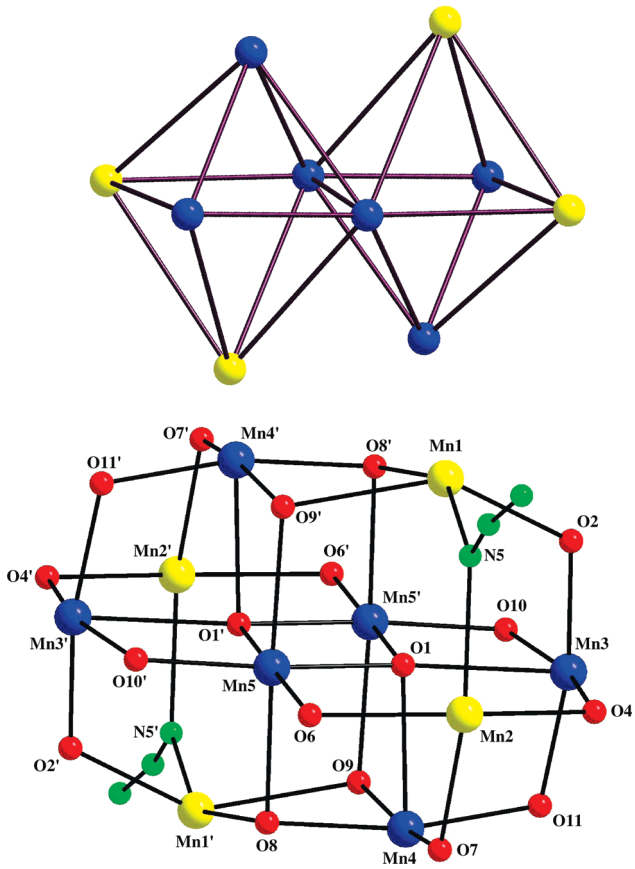

Figure 4. (top) Mn_{10} topology of **3**, emphasizing the fused-bioctahedral description. Dark purple lines indicate the $Mn^{2+}\cdots Mn^{3+}$ and $Mn^{3+}\cdots Mn^{3+}$ vectors. (bottom) The complete $[Mn_{10}(\mu_4\text{-}O)_2(\mu\text{-}N_3)_2(\mu_3\text{-}OR)_4(\mu\text{-}OR)_{12}]^{4+}$ core. Color scheme: Mn^{II}, yellow; Mn^{III}, blue; O, red; N, green.

Table 5. Bond Valence Sum (BVS)[a,b] Calculations for Mn and Selected Oxygen Atoms in **3**

atom	Mn^{II}	Mn^{III}	Mn^{IV}
Mn1	1.97	1.85	1.87
Mn2	1.87	1.75	1.77
Mn3	3.26	3.01	3.12
Mn4	3.16	2.92	3.03
Mn5	3.10	2.84	2.98
	BVS	Assignment	Group
O1	1.67[c]	O^{2-} (μ_4)	
O2	1.78	RO^- (μ)	pdmH$^-$
O3	1.08	ROH	pdmH$^-$
O4	1.80	RO^- (μ)	pdmH$^-$
O5	1.12	ROH	pdmH$^-$
O6	1.79	RO^- (μ)	thme^{3-}
O7	1.81	RO^- (μ)	thme^{3-}
O8	1.91	RO^- (μ_3)	thme^{3-}
O9	1.83	RO^- (μ_3)	thme^{3-}
O10	1.87	RO^- (μ)	thme^{3-}
O11	1.87	RO^- (μ)	thme^{3-}

[a] See footnote a of Table 3. [b] See footnote b of Table 3. [c] Including the long Mn1−O1 (2.811 Å) and Mn2−O1 (2.678 Å) bonds.

formed on powdered polycrystalline samples of **1**−**4**, restrained in eicosane to prevent torquing, in a 1 kG (0.1 T) field and in the 5.0–300 K range. The obtained data are shown as a $\chi_M T$ versus T plot in Figure 7. The magnetic

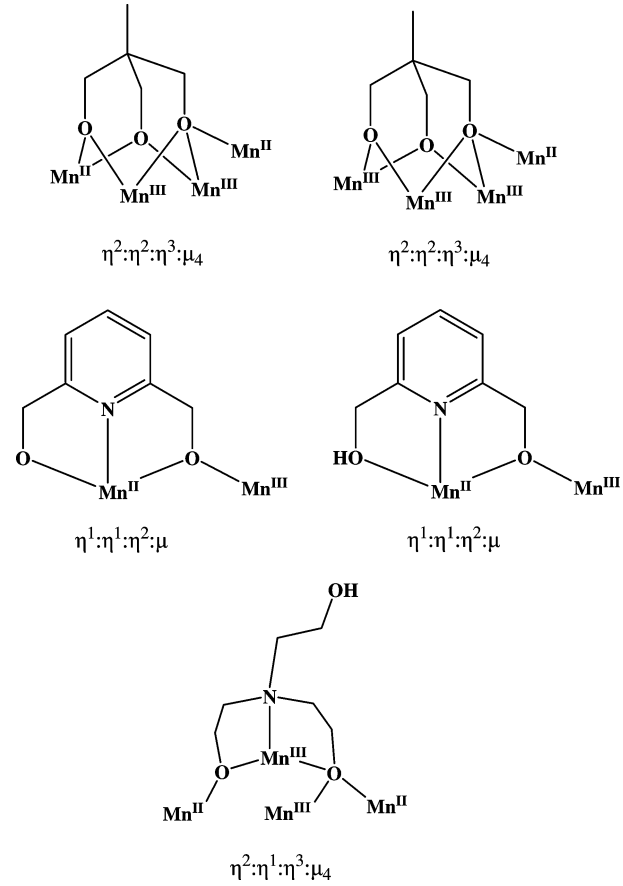

Figure 5. Coordination/bridging modes of the alcohol-based ligands in complexes **3** and **4**.

data for **1** and **2** are almost identical, and therefore, only those of the former will be discussed; the magnetic data for **2** are available in the Supporting Information.

$\chi_M T$ for **1**·MeCN steadily increases from 53.78 cm^3 K mol^{-1} at 300 K to a maximum of 231.56 cm^3 K mol^{-1} at 10 K, before dropping to 220.23 cm^3 K mol^{-1} at 5.0 K. The 300 K value is much larger than the spin-only ($g = 2$) value of 35.5 cm^3 K mol^{-1} for four Mn^{II} and six Mn^{III} noninteracting ions, indicating the presence of dominant ferromagnetic exchange interactions within **1** and suggesting a very large ground-state spin (S) value. The 10.0 K value is consistent with an $S = 22$ ground state, the maximum possible, and a g factor slightly less than 2.0, as expected for a Mn^{II}/Mn^{III} complex; the spin-only ($g = 2$) value for an $S = 22$ state is 253 cm^3 K mol^{-1}. The sharp decrease at the lowest temperatures (<10.0 K) is assigned to Zeeman effects, zero-field splitting (ZFS), and/or weak intermolecular interactions. Given the size of the Mn_{10} cation and the resulting number of inequivalent exchange constants, it is not possible

(55) Liu, S.- X.; Lin, S.; Lin, B.- Z.; Lin, C.- C.; Huang, J.- Q. *Angew. Chem., Int. Ed.* **2001**, *40*, 1084.
(56) Eppley, H. J.; Aubin, S. M. J.; Streib, W. E.; Bollinger, J. C.; Hendrickson, D. N.; Christou, G. *Inorg. Chem.* **1997**, *36*, 109.
(57) Jones, L. F.; Rajaraman, G.; Brockman, J.; Murugescu, M.; Sanudo, E. C.; Raftery, J.; Teat, S. J.; Wernsdorfer, W.; Christou, G.; Brechin, E. K.; Collison, D. *Chem.—Eur. J.* **2004**, *10*, 5180.
(58) Hagen, K.; Armstrong, W. H. *J. Am.Chem. Soc.* **1989**, *111*, 774.
(59) (a) Wittick, L. M.; Murray, K. S.; Moubaraki, B.; Batten, S. R.; Spiccia, L.; Berry, K. J. *Dalton Trans.* **2004**, 1003. (b) Yoo, J.; Yamaguchi, A.; Nakano, M.; Krzystek, J.; Streib, W. E.; Brunel, L.- C.; Ishimoto, H.; Christou, G.; Hendrickson, D. N. *Inorg. Chem.* **2001**, *40*, 4604. (c) Lecren, L.; Li, Y.- G.; Wernsdorfer, W.; Roubeau, O.; Miyasaka, H.; Clérac, R. *Inorg. Chem. Commun.* **2005**, *8*, 626.

Table 6. Structural Types and Ground State *S* Values for Decanuclear Mn Clusters

complex[a,b]	core	*S*	ref
$[Mn_{10}(OH)_3(phth)_9(bpy)_6]^{2-}$ [c]	$[Mn_{10}(\mu_3\text{-}OH)_3(\mu\text{-}OR)_6]^{11+}$	2	48
$[Mn_{10}(O_2CPh)_{12}(pao)_6(paoH)_2]^{2+}$ [c]	$[Mn_{10}(\mu\text{-}OR)_{10}]^{10+}$	0	49
$[Mn_{10}O_4Cl_{12}(biphen)_4]^{4-}$ [d]	$[Mn_{10}(\mu_4\text{-}O)_4(\mu_3\text{-}Cl)_4(\mu\text{-}Cl)_4(\mu\text{-}OR)_8]$	14	50
$[Mn_{10}O_4(N_3)_4(hmp)_{12}]^{2+}$ (**1**/**2**) [e]	$[Mn_{10}(\mu_4\text{-}O)_4(\mu_3\text{-}N_3)_4(\mu\text{-}OR)_{12}]^{2+}$	22	t.w.
$[Mn_{10}O_4Br_4(amp)_6(ampH_2)_3(ampH_3)]^{3+}$ [e]	$[Mn_{10}(\mu_4\text{-}O)_4(\mu_3\text{-}Br)_4(\mu\text{-}OR)_{12}]^{2+}$	22	51
$[Mn_{10}O_2(N_3)_6(pdmH)_4(thme)_4]$ (**3**) [e]	$[Mn_{10}(\mu_4\text{-}O)_2(\mu\text{-}N_3)_2(\mu_3\text{-}OR)_4(\mu\text{-}OR)_{12}]^{4+}$	0	t.w.
$[Mn_{10}O_2Cl_8(thme)_6]^{2-}$ [f]	$[Mn_{10}(\mu_6\text{-}O)_2(\mu\text{-}OR)_{18}]^{6+}$	n.r.	52
$\{[Mn_{10}O_2(O_2CMe)_{13}(pd)_6(py)_2]^{-}\}_4$ [f]	$[Mn_{10}(\mu_3\text{-}O)_2(\mu\text{-}OR)_{17}]^{7+}$	4	53
$[Mn_{10}(2\text{-}dmpshz)_{10}(py)_{10}]$ [g]	$[Mn_{10}(\mu\text{-}NN)_{10}]^{20+}$	2	54
$[Mn_{10}(bzshz)_{10}(MeOH)_{10}]$ [g]	$[Mn_{10}(\mu\text{-}NN)_{10}]^{20+}$	2	55
$[Mn_{10}O_8(O_2CPh)_6(pic)_8]$ [g]	$[Mn_{10}(\mu_4\text{-}O)_2(\mu_3\text{-}O)_6]^{14+}$	0	56
$[Mn_{10}O_6(OH)_2F_8(bta)_8(py)_8]$ [g]	$[Mn_{10}(\mu_3\text{-}O)_6(\mu_3\text{-}OH)_2(\mu\text{-}F)_4(\mu\text{-}NN)_8]^{4+}$	0	57
$[Mn_{10}O_4(OH)_2(O_2CMe)_8(hmp)_8]^{4+}$ [g]	$[Mn_{10}(\mu_3\text{-}O)_4(\mu_3\text{-}OH)_2(\mu_3\text{-}OR)_2(\mu\text{-}OR)_6]^{12+}$	0	20a
$[Mn_{10}O_{14}(tren)_6]^{8+}$ [h]	$[Mn_{10}(\mu_3\text{-}O)_8(\mu\text{-}O)_6]^{8+}$	0	58

[a] Counterions and solvate molecules are omitted. [b] Abbreviations: n.r. = not reported; t.w. = this work; $phthH_2$ = phthalic acid; bpy = 2,2′-bipyridine; $paoH_2$ = 2-pyridinealdoxime; pdH_2 = 1,3-propanediol; py = pyridine; $ampH_3$ = 2-amino-2-methyl-1,3-propanediol; $biphenH_2$ = 2,2′-biphenol; $2\text{-}dmpshzH_3$ = N-(2,2-dimethylpropanoyl)salicylhydrazine; bzshz = N-phenylsalicylhydrazine; picH = picolinic acid; btaH = benzotriazole; tren = tris(2-aminoethyl)amine. [c] Mn^{II}_{10}. [d] $Mn^{II}_6Mn^{III}_4$. [e] $Mn^{II}_4Mn^{III}_6$. [f] $Mn^{II}_2Mn^{III}_8$. [g] Mn^{III}_{10}. [h] $Mn^{III}_4Mn^{IV}_6$.

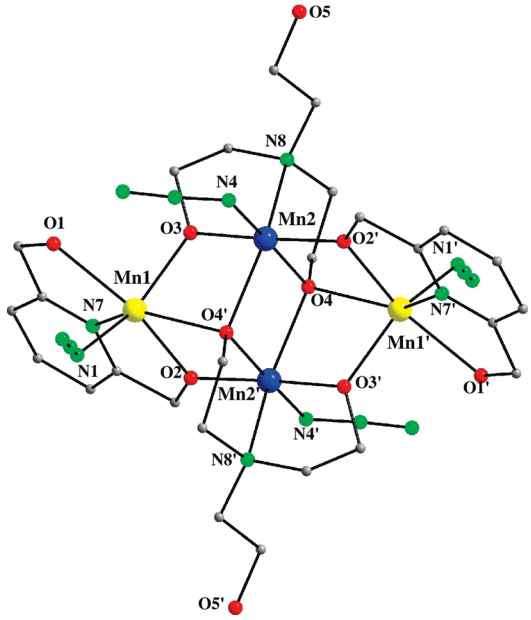

Figure 6. Labeled PovRay representation of the structure of **4**, with the hydrogen atoms omitted for clarity. Color scheme: Mn^{II}, yellow; Mn^{III}, blue; O, red; N, green; C, gray.

Table 7. Selected Interatomic Distances (Å) and Angles (deg) for **4**[a]

parameter		parameter	
Mn(1)···Mn(1′)	5.834(5)	Mn(1)···Mn(2′)	3.314(2)
Mn(1)···Mn(2)	3.372(2)	Mn(2)···Mn(2′)	3.267(2)
Mn(1)−O(1)	2.319(2)	Mn(2)−O(2′)	1.902(1)
Mn(1)−O(2)	2.161(1)	Mn(2)−O(3)	1.914(1)
Mn(1)−O(3)	2.084(1)	Mn(2)−O(4)	1.969(1)
Mn(1)−O(4′)	2.388(1)	Mn(2)−O(4′)	2.240(1)
Mn(1)−N(1)	2.128(2)	Mn(2)−N(4)	1.975(2)
Mn(1)−N(7)	2.227(2)	Mn(2)−N(8)	2.382(2)
Mn(1)−O(2)−Mn(2′)	109.0(6)	Mn(1)−O(4′)−Mn(2′)	98.5(5)
Mn(1)−O(3)−Mn(2)	114.9(6)	Mn(2)−O(4′)−Mn(2′)	101.6(5)
Mn(1)−O(4′)−Mn(2)	93.4(5)		

[a] Primed and unprimed atoms are related by symmetry.

to apply the Kambe method[60] to determine the individual pairwise Mn_2 exchange interaction parameters. We instead used theoretical DFT and ZILSH calculations to obtain

(60) Kambe, K. *J. Phys. Soc. Jpn.* **1950**, *5*, 48.

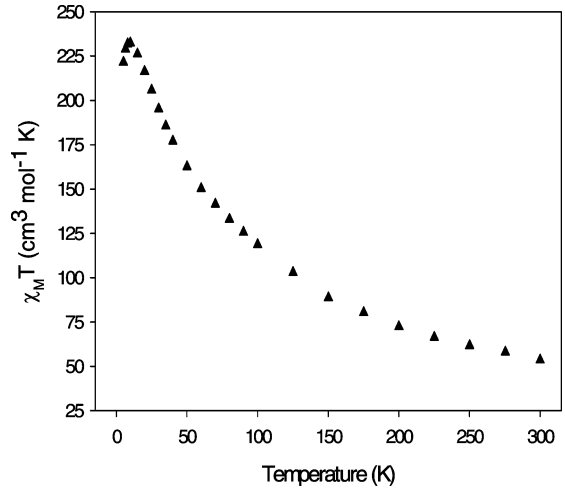

Figure 7. Plot of $\chi_M T$ vs *T* for complex **1**·MeCN in a 1 kG dc field.

estimates of the exchange constants (vide infra) and concentrated experimental efforts on characterizing the ground-state spin, *S*, and the zero-field splitting parameter, *D*.

To confirm the indicated $S = 22$ ground-state of **1**·MeCN and to determine *D*, magnetization (*M*) versus dc field measurements were made on restrained samples in the magnetic field (*H*) and temperature ranges of 1–50 kG and 1.8–10.0 K, respectively. The resulting data are shown in Figure 8 as a reduced magnetization ($M/N\mu_B$) versus H/T plot, where *N* is Avogadro's number and μ_B is the Bohr magneton. The various isofield lines are virtually superimposed, indicating essentially no zero-field splitting (ZFS) within the ground state, and the saturation value of $M/N\mu_B \approx 44$ is consistent with a spin value of $S = 22$. The data were fit by matrix diagonalization, using the program MAGNET,[28] to a model that assumes only that the ground-state is populated at these temperatures and magnetic fields, includes isotropic Zeeman interactions and axial zero-field splitting ($D\hat{S}_z^2$), and incorporates a full powder average. The corresponding spin Hamiltonian is given by eq 7, where $\hat{S}_z$ is the easy-axis spin operator, and μ_0

$$\mathbf{H} = D\hat{S}_z^2 + g\mu_B\mu_0\hat{S}\cdot H \qquad (7)$$

is the vacuum permeability. The last term in eq 7 is the

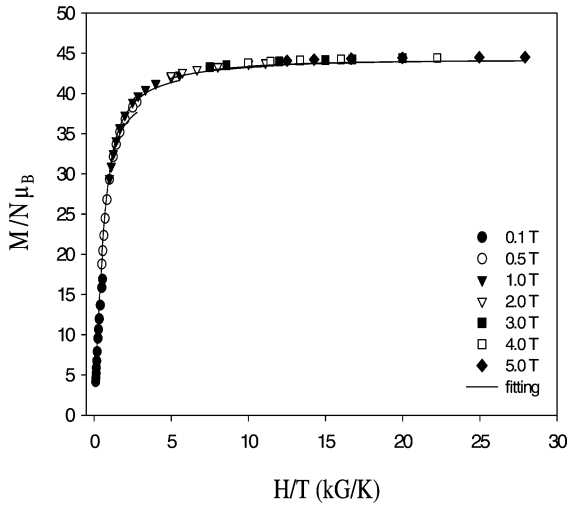

Figure 8. Plot of reduced magnetization ($M/N\mu_B$) vs H/T for complex **1**·MeCN at applied fields of 0.1–5.0 T and in the 1.8–10 K temperature range. The solid lines are the fit of the data; see the text for the fit parameters.

Zeeman energy associated with an applied magnetic field. The best fit is shown as the solid lines in Figure 8 and was obtained with $S = 22$, $g = 2.00$, and $D = -0.011$ cm^{-1}, thus confirming a very high-spin ground-state with little or no anisotropy ($D \approx 0$). The latter was anticipated from the high (isotropic/cubic) symmetry of the molecule because, although Mn^{III} ions have significant single-ion anisotropy, the molecular anisotropy is the tensorial sum of the single-ion values, and this sum should be essentially zero given the cubic symmetry and the resulting orientations of the six Mn^{III} Jahn–Teller axes.[7,51,61] Of course, disorder in the ClO_4^- anions and MeCN solvent of crystallization can lower slightly the local site-symmetry of a molecule, so it is not expected that the D value must be exactly zero. Alternative fits with $S < 22$ were rejected because they gave unreasonable values of g and D.

As we have described before on multiple occasions,[8,15,16b,21a,40,42,62] ac susceptibility studies are a powerful complement to dc studies as an alternative and independent means of determining the ground-state of a system; they also preclude any complications arising from low-lying excited states in the presence of an applied dc field. Alternating current susceptibility data were collected in the 1.8–15 K range using a 3.5 G ac field oscillating at frequencies in the 50–1000 Hz range. If the magnetization vector can relax fast enough to keep up with the oscillating field, then there is no imaginary (out-of-phase) susceptibility signal (χ''_M), and the real (in-phase) susceptibility (χ'_M) is equal to the dc

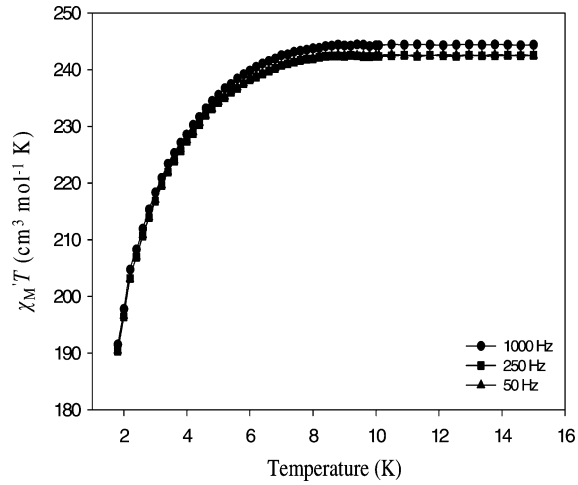

Figure 9. Plot of the in-phase ac susceptibility signal as χ'_MT vs T for complex **1**·MeCN at the indicated frequencies.

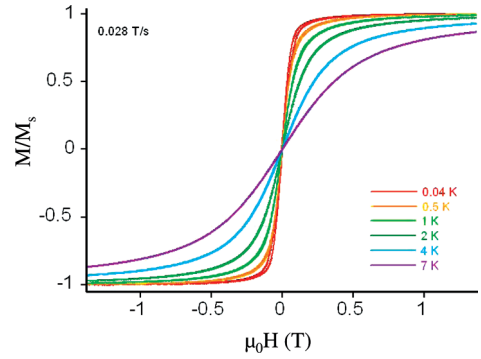

Figure 10. Magnetization vs applied dc field scans for a single-crystal of complex **1**·MeCN at the indicated field sweep rate and temperatures. The magnetization is normalized to its saturation value, M_S.

susceptibility. For **1**·MeCN, the in-phase χ'_MT signal is temperature-independent at about 244 cm^3 K mol^{-1} from 15 K down to about 8 K (Figure 9), consistent with a well isolated (vs kT) ground-state of $S = 22$ and $g \sim 1.96$, in agreement with the dc magnetization fit. At lower temperatures, χ'_MT decreases slightly, and we assign this to the weak intermolecular interactions, both dipolar and superexchange in nature. We conclude that complex **1** is confirmed to have an $S = 22$ ground state.

Complex **1** did not exhibit an out-of-phase ac magnetic susceptibility signal down to 1.8 K, indicating that it does not exhibit a barrier large enough (vs kT) to show the superparamagnet-like slow relaxation of its magnetization vector, that is, it is not a SMM. This is consistent with the cubic (T) symmetry and the absence of anisotropy. This was also reflected in single-crystal magnetization versus dc field scans down to 0.04 K, with the field applied in turn along three perpendicular axes of the crystal.[29] All gave essentially superimposable scans, as shown for one field direction in Figure 10. There is clearly no hysteresis observed. The combined results confirm an isotropic crystal and a fast magnetization relaxation even at 0.04 K, consistent with $D \approx 0$.

The $S = 22$ ground-state for **1** (and **2**) is the maximum for a $Mn^{III}_6Mn^{II}_4$ species, thus indicating that all interactions are ferromagnetic. This is consistent with the presence of

(61) (a) Tsai, H.- L.; Wang, S.; Folting, K.; Streib, W. E.; Hendrickson, D. N.; Christou, G. *J. Am. Chem. Soc.* **1995**, *117*, 301. (b) King, P.; Wernsdorfer, W.; Abboud, K. A.; Christou, G. *Inorg. Chem.* **2005**, *44*, 8659. (c) Aromi, G.; Knapp, M. J.; Claude, J.- P.; Huffman, J. C.; Hendrickson, D. N.; Christou, G. *J. Am. Chem. Soc.* **1999**, *121*, 5489.
(62) For some representative references, see:(a) Soler, M.; Wernsdorfer, W.; Folting, K.; Pink, M.; Christou, G. *J. Am. Chem. Soc.* **2004**, *126*, 2156. (b) Sanudo, E. C.; Wernsdorfer, W.; Abboud, K. A.; Christou, G. *Inorg. Chem.* **2004**, *43*, 4137. (c) Tasiopoulos, A. J.; Wernsdorfer, W.; Abboud, K. A.; Christou, G. *Inorg. Chem.* **2005**, *44*, 6324. (d) Murugesu, M.; Raftery, J.; Wernsdorfer, W.; Christou, G.; Brechin, E. K. *Inorg. Chem.* **2004**, *43*, 4203.

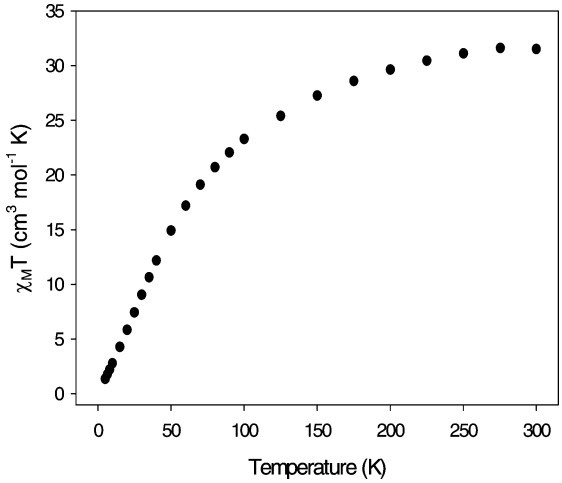

Figure 11. Plot of $\chi_M T$ vs T for complex **3** in a 1 kG dc field.

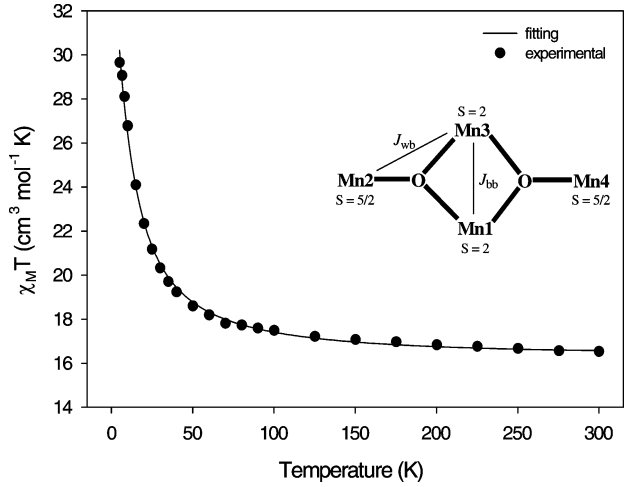

Figure 12. Plot of $\chi_M T$ vs T for complex **4** in a 1 kG dc field. The solid line is the fit of the data to the theoretical expression; see the text for the fit parameters. (inset) Definition of the exchange parameters.

end-on-bridging N_3^- groups on the Mn^{III}_3 faces of the central octahedron, and the fact that each $Mn^{II}\cdots Mn^{III}$ pair is bis(monoatomically)-bridged by two separate O atoms with rather acute Mn−O−Mn angles (∼101–105°); both situations are known to yield ferromagnetic interactions.[18,20,24] Note that such a high S value is extremely rare; in fact, it is the fourth-highest in Mn chemistry to date[7–10] and very similar in magnitude to the $S = 23$ for an Fe_{14} cluster, the largest in Fe chemistry.[63]

For complex **3**, the obtained dc data are shown as $\chi_M T$ versus T in Figure 11. $\chi_M T$ rapidly decreases from 31.51 cm^3 K mol^{-1} at 300 K to 1.35 cm^3 K mol^{-1} at 5.0 K. In contrast to **1**, the 300 K value for **3** is slightly less than the spin-only ($g = 2$) value of 35.5 cm^3 K mol^{-1} for four Mn^{II} and six Mn^{III} noninteracting ions, indicating the presence of dominant antiferromagnetic exchange interactions and strongly suggesting an $S = 0$ ground-state spin for **3**. Again, the high nuclearity and low symmetry of the complex make it extremely difficult to evaluate the various exchange parameters. The $S = 0$ ground-state was supported by the ac in-phase $\chi'_M T$ versus T data, which show a steady decrease below 15 K and are clearly heading for $\chi'_M T \approx 0$ at 0 K (see Supporting Information).

For complex **4**, $\chi_M T$ continuously increases from 16.53 cm^3 K mol^{-1} at 300 K to 29.66 cm^3 K mol^{-1} at 5.0 K (Figure 12). The 300 K value is appreciably larger than the spin-only ($g = 2$) value of 14.75 cm^3 K mol^{-1} for two Mn^{II} and two Mn^{III} noninteracting ions, indicating the presence of dominant ferromagnetic exchange interactions and suggesting a large ground-state spin (S) value. The 5.0 K value is still steeply increasing, suggesting an $S = 8$ or 9 ground state; the spin-only ($g = 2$) values for $S = 8$ or 9 are 36 and 45 cm^3 K mol^{-1}, respectively. Previous Mn_4 complexes with a $[Mn_4(\mu_3\text{-OR})_2(\mu\text{-OR})_4]^{4+}$ rhombus-like core have always reached a $\chi_M T$ maximum at around 15–10 K before then decreasing at lower temperatures because of zero-field splitting, Zeeman effects, and so forth.[20b,d,21b,24a,25a,59]

The $\chi_M T$ versus T data were least-squares-fit to a theoretical expression derived assuming approximate C_{2v} symmetry for the Mn_4 core. This requires two exchange parameters, J_{wb} and J_{bb}, defined in the inset to Figure 12. The corresponding Heisenberg spin Hamiltonian (eq 7) can be converted to the equivalent one in eq 8 using Kambe vector coupling method,[60] where $\hat{S}_A = \hat{S}_1 + \hat{S}_3$, $\hat{S}_B = \hat{S}_2 + \hat{S}_4$, and $\hat{S}_T = \hat{S}_A + \hat{S}_B$.

$$\hat{H} = -2J_{wb}(\hat{S}_1\cdot\hat{S}_2 + \hat{S}_1\cdot\hat{S}_4 + \hat{S}_2\cdot\hat{S}_3 + \hat{S}_3\cdot\hat{S}_4) - 2J_{bb}\hat{S}_1\cdot\hat{S}_3 \quad (7)$$

$$\hat{H} = -J_{wb}(\hat{S}_T^{\,2} - \hat{S}_A^{\,2} - \hat{S}_B^{\,2}) - J_{bb}(\hat{S}_A^{\,2} - \hat{S}_1^{\,2} - \hat{S}_3^{\,2}) \quad (8)$$

$$E(S_T, S_A, S_B) = -J_{wb}[S_T(S_T+1) - S_A(S_A+1) - S_B(S_B+1)] - J_{bb}[S_A(S_A+1)] \quad (9)$$

The corresponding eigenvalue expression is given in eq 9. There are a total of 110 possible S_T states ranging in value from 0 to 9, where S_T is the total spin of the Mn_4 cluster. This eigenvalue expression and the Van Vleck equation were used to derive a theoretical $\chi_M T$ versus T expression for **4**, and this was used to least-squares-fit the experimental data. The fit (solid line in Figure 12) gave $J_{wb} = +0.03$ cm^{-1}, $J_{bb} = +1.19$ cm^{-1}, and $g = 1.96$, with temperature-independent paramagnetism (TIP) fixed at 600×10^{-6} cm^3 mol^{-1}. These values identify a $|S_T, S_A, S_B\rangle = |9, 4, 5\rangle$ ground-state for **4** but with many low-lying excited states; the first and second excited states are the $|8, 4, 4\rangle$ and $|7, 4, 3\rangle$ states at 0.25 and 0.49 cm^{-1} above the ground state, respectively. As a result, it is possible that within the fit uncertainties and the approximations for the model the ground-state might be the $S = 8$ or even the $S = 7$ state, although we note that an $S = 9$ ground-state is well within precedent in other Mn_4 compounds with the same core.

To probe the ground-state further, we attempted fits of magnetization data collected in the 1–70 kG and 1.8–10.0 K ranges but could get no acceptable fits, even using just the lowest temperature data and the selected field ranges. This is completely consistent with very low-lying excited

(63) Low, D. M.; Jones, L. F.; Bell, A.; Brechin, E. K.; Mallah, T.; Riviere, E.; Teat, S. J.; McInnes, E. J. L. *Angew. Chem., Int. Ed.* **2003**, *42*, 3781.

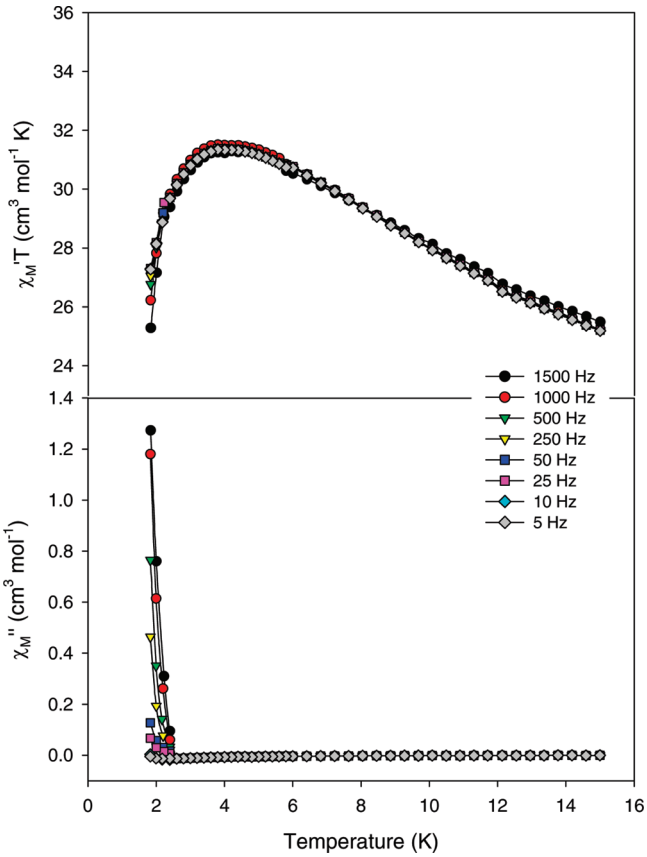

Figure 13. Plot of the in-phase (χ'_M) (as $\chi'_M T$, top) and out-of-phase (χ''_M, bottom) ac susceptibility signals of complex **4** in a 3.5 G field oscillating at the indicated frequencies.

states as indicated by the susceptibility fits because the attempted magnetization fits assumed only the ground-state was populated and this was clearly not the case. As an additional probe, we collected ac susceptibility data in a 3.5 G ac field oscillating at frequencies in the 5–1500 Hz range. The in-phase $\chi'_M T$ vs T data are shown in Figure 13 (top) and show a continuous increase below 15 K consistent with decreasing population of low-lying excited states with S smaller than that of the ground state. Below 5 K, the plot plateaus and decreases as a result of intermolecular interactions (via the H-bonding network) and then slow magnetization relaxation, precluding a clear determination of how high the $\chi'_M T$ versus T plot would rise down to 1.8 K. Nevertheless, on the basis of data above 5 K, it is clearly heading for values consistent with an $S = 8$ or 9 ground state (spin-only values of 36 and 45 cm^3 K mol^{-1}). Both $S = 8$ and 9 ground states have been previously observed for other clusters with a $[Mn_4(\mu_3\text{-OR})_2(\mu\text{-OR})_4]^{4+}$ rhombus-like core.[20b,d,21b,24a,25a,59] On the basis of the combined dc and ac studies, we thus conclude that complex **4** likely possesses an $S = 9$ ground-state with a very low-lying $S = 8$ excited state, but we cannot rule out the possibility that the order is reversed.

Below ~2.5 K, the decrease in the $\chi'_M T$ versus T plot is frequency dependent, and there is a concomitant appearance of a frequency-dependent out-of-phase χ''_M signal (Figure 13, bottom), whose peak is below the operating minimum of our SQUID magnetometer. Such behavior is indicative (but not diagnostic[64]) of the superparamagnetic-like properties of a SMM, as has been confirmed for a number of Mn_4 complexes of this structural type.[20b,d,21b,24a,25a,59]

The only weakly ferromagnetic exchange coupling in **4** ($J_{wb} = 0.03$ cm^{-1}, $J_{bb} = 1.19$ cm^{-1}) is unusual for this Mn_4 family, for which the interactions are usually more strongly ferromagnetic. However, there is also a more extreme example, $[Mn^{II}_2Mn^{III}_2(hmp)_6(hmpH)_2]^{2+}$ reported by Clerac and co-workers,[20d] that was found to exhibit intramolecular antiferromagnetic J_{wb} interactions and a resulting small ($S = 1$) ground state. In addition, it has a very weak J_{bb} (+0.17 cm^{-1}) clearly related to its larger $Mn^{III}-OR-Mn^{III}$ angles (102.9°) and longer $Mn^{III}\cdots Mn^{III}$ separations (3.353 Å) compared with previous $Mn^{III}_2Mn^{II}_2$ complexes (average values: J_{bb} = 8–9 cm^{-1}, $Mn^{III}-OR-Mn^{III}$ = ~99°, $Mn^{III}\cdots Mn^{III}$ = 3.150–3.230 Å). The $Mn^{III}-OR-Mn^{III}$ angles (101.7°) and the $Mn^{III}\cdots Mn^{III}$ distance (3.267 Å) in **4** fall into an intermediate range rationalizing a weakly ferromagnetic interaction and the experimentally observed $J_{bb} = +1.19$ cm^{-1}. The J_{wb} exchange parameters have always been weak and either side of zero (−0.92 to 1.24 cm^{-1}) as expected for $Mn^{II}-Mn^{III}$ interactions.[65]

Theoretical Studies. To provide independent estimates of the constituent exchange interaction constants and spin couplings, theoretical calculations were carried out on a complete complex **1** using the semiempirical ZILSH method[30] and on a fragment modeling of the $Mn^{II}-Mn^{III}$ interactions with DFT calculations (vide infra). ZILSH calculations were performed on 46 spin components so that estimates of all parameters in eq 2 could be obtained (E_0 and 45 pairwise exchange constants). The components used were the ones with all unpaired spins aligned parallel ("high spin", HS) and all components with unpaired spin on two metal ions reversed relative to all others (e.g., unpaired spin on Mn1 and Mn2 reversed, those on Mn1 and Mn3 reversed, etc.). Energies and local spin densities of the Mn ions for each component are presented in the Supporting Information, Table S1. To summarize these results, the HS component is quite low in energy relative to other components; the lowest energy components are those with spins of pairs of Mn^{2+} ions reversed, stabilized by about 14 cm^{-1} relative to the high spin component. This indicates that interactions between Mn^{2+} and Mn^{3+} ions might be slightly antiferromagnetic, but other magnetic interactions in the complex must be strongly ferromagnetic. The spin densities are close to the formal values of five or four expected for high-spin Mn^{2+} (d^5) and Mn^{3+} (d^4) ions, respectively, but are reduced below these numbers by spin delocalization, as found with ZILSH for other complexes.[30,66] The signs of the local spin densities

(64) Intermolecular interactions and phonon bottlenecks can also give such signals; for representative references, see:(a) Chakov, N. E.; Wernsdorfer, W.; Abboud, K. A.; Christou, G. *Inorg. Chem.* **2004**, *43*, 5919. (b) Mishra, A.; Tasiopoulos, A. J.; Wernsdorfer, W.; Abboud, K. A.; Christou, G. *Inorg. Chem.* **2007**, *46*, 3105.

(65) Stamatatos, Th. C.; Christou, G. *Phil. Trans. R. Soc. A* **2008**, *366*, 113; and references therein.

(66) (a) Stamatatos, Th. C.; Christou, A. G.; Jones, C. M.; O'Callaghan, B. J.; Abboud, K. A.; O'Brien, T. A.; Christou, G. *J. Am. Chem. Soc.* **2007**, *129*, 9840. (b) Cañada-Vilalta, C.; O'Brien, T. A.; Brechin, E. K.; Pink, M.; Davidson, E. R.; Christou, G. *Inorg. Chem.* **2004**, *43*, 5505.

Table 8. Computational Results for Fragment Complex $[Mn^{II}Mn^{III}O(hmp)(hmpH)_3(OH)(N_3)_2]^-$

component[a]	quantity	ZILSH	B3LYP/I	B3LYP/II
HS	E	20.7[c] (−357.18975563)[d]	0.0[c] (−4230.55932839)[d]	0.0[c] (−4232.71532574)[d]
	$\langle \hat{S}_1 \cdot \hat{S}_2 \rangle$[e]	4.724		
	M_I[f]	4.88	4.77	4.77
	M_2	3.92	3.88	3.88
AF[b]	E	0.0[c]	121.6[c]	8.6[c]
	$\langle \hat{S}_1 \cdot \hat{S}_2 \rangle$	−4.691		
	M_1	4.85	4.73	4.76
	M_2	−3.92	−3.86	−3.87
	J (cm^{-1})	−1.1 (−0.3)[g]	+6.5	+0.5

[a] Component with all unpaired spins aligned. [b] Component with unpaired spins on Mn2 (Mn^{3+}) reversed relative to those on Mn1. [c] Relative energy (cm^{-1}). [d] Absolute energy (a.u.). [e] Spin coupling between Mn1 and Mn2 computed with ZILSH method. [f] Local z component of spin for Mn1. [g] From ZILSH calculations on full complex. See text for discussion.

indicate the relative directions of the spin moments of the manganese ions and show that correct spin distributions were obtained for all spin components considered.

Exchange constants were obtained for **1** from the data of Supporting Information, Table S1 by simultaneous solution of eqs 2. Considering first the central octahedron of six Mn^{III} ions, the interactions among these ions are all equivalent and strongly ferromagnetic with values of $J_{III-III} = +26.1$ cm^{-1}. These spins are thus aligned parallel. Each Mn^{II} ion caps a Mn^{III}_3 face of the octahedron and thus has equivalent interactions with three Mn^{III} ions and no other first-neighbor interactions. Because the Mn^{III} ions are all parallel, the spins of all Mn^{II} ions would align parallel to those of the Mn^{III} ions if the interactions were ferromagnetic, leading to a ground-state spin of 22. If the interactions were antiferromagnetic, the spins of the Mn^{II} and Mn^{III} ions would align antiparallel leading to a ground-state spin of 2. Spin frustration is not a possibility in either case, and the ground-state spin is determined solely by the sign of the exchange constant for the $Mn^{II}-Mn^{III}$ interactions.

The ZILSH calculations indicate that all exchange constants other than those between nearest-neighbor Mn^{III} ions are very small, less than one cm^{-1} in magnitude, including the nearest neighbor $Mn^{II}-Mn^{III}$ interactions. The latter were found to be very slightly antiferromagnetic, with values of $J_{II-III} = -0.3$ cm^{-1}, which would yield an $S = 2$ ground-state stabilized by ~ 4 cm^{-1} from an $S = 3$ first excited state. This is in clear disagreement with the experimental determination of a well-isolated $S = 22$ ground state. If J_{II-III} was even slightly ferromagnetic, the $S = 22$ state would be the ground state. Thus, even a very small error (on the order of one cm^{-1}) in the $Mn^{II}-Mn^{III}$ exchange constant would have a direct impact on the spin of the ground state. We observed a similar situation in the Mn^{II}/Mn^{III} complex $[Mn_{12}(O_2CMe)_{14}(mda)_8]$:[24a] ZILSH calculations indicated that certain $Mn^{II}-Mn^{III}$ interactions were very slightly antiferromagnetic, but this was inconsistent with the experimental magnetic studies of the complex. Refinement of exchange constants with more accurate DFT calculations showed that these interactions were in fact slightly ferromagnetic, in accord with experimental studies. Thus, a similar strategy was employed in the present work.

The complex is too large to be treated with DFT by considering 46 spin components and solving for all parameters in eq 2, as was done with the more efficient ZILSH method, but the ferromagnetic $Mn^{III}-Mn^{III}$ interactions are strong enough that small errors in their value will not influence the spin of the ground state. Only the $Mn^{II}-Mn^{III}$ exchange constants need to be refined, and these interactions are all equivalent. A model cluster comprising one pair of contiguous Mn^{II} and Mn^{III} ions and their associated ligands can be used for this purpose; we have previously used this approach to refine exchange constants with DFT calculations in large complexes, [24a] as have other authors.[38] The model cluster used consisted of Mn1 and Mn2 (see Figure 1 for numbering scheme) and their associated ligands, including terminal hmp^- ligands for each metal and azide and oxide ligands for Mn2. The two metals are bridged by an oxide ligand and the OR^- moiety of an hmp^- ligand. The external (nonbridging) oxide and hmp^- ligands were protonated to compensate for removal of strongly electropositive metal ions that also interact with these ligands in the full cluster and to ensure that the charge on the model cluster was not excessively negative. The positions of the added protons were optimized using the MM+ forcefield with the Hyperchem program,[67] while keeping all other atoms in fixed positions. The resulting model cluster thus has a formula $[Mn^{II}Mn^{III}O(hmp)(hmpH)_3(OH)(N_3)_2]^-$.

Computational results obtained for the model fragment with ZILSH calculations and DFT calculations with basis sets I and II are given in Table 8. The z components of spin obtained for the Mn ions indicate that correct spin distributions were achieved for both components with all three methods. ZILSH calculations again give an antiferromagnetic exchange constant, with a magnitude in reasonable agreement with that found for this interaction in the full complex (−1.1 cm^{-1} vs −0.3 cm^{-1}). The magnetic interaction between Mn^{2+} and Mn^{3+} ions in the full complex is thus represented well by the model cluster. DFT calculations with the smaller basis set (basis set I in Table 8) indicate that the interaction is in fact ferromagnetic, with a value of $J = +6.5$ cm^{-1}. This value was obtained with the energy difference given in Table 8 and spin couplings obtained with ZILSH calculations on the model cluster. When used in place of $J_{II-III} = -0.3$ cm^{-1} found with ZILSH calculations, spin eigenstate calculations show that the ground-state has $S = 22$ and is stabilized relative to the first excited-state with $S = 21$ by about 73 cm^{-1}.

Repeating the DFT calculations with the larger basis set II also gives a ferromagnetic exchange constant but with a much smaller magnitude of +0.5 cm^{-1}. The $S = 22$ ground-

(67) *Hyperchem*-Release 5.1 Pro for Windows; Hypercube, Inc.: Gainesville, FL, 1997.

state is stabilized relative to the $S = 21$ excited-state by only about 5 cm^{-1} with this exchange constant, which appears to be too small; a simple application of the Boltzmann distribution to the two states with this energy difference at 15 K gives a relative ground-state population of about 63%. This disagrees with the ac magnetic susceptibility studies (vide supra), which showed the ground-state to be well isolated in this temperature range. The energy difference of 73 cm^{-1} obtained with the smaller basis set appears to be in better agreement, as the relative ground-state population at 15 K with this energy difference is virtually 100%. It is interesting to note that DFT calculations with a smaller basis set give results that are more consistent with experiment. The energy difference of 73 cm^{-1} provides a reasonable upper bound of +6.5 cm^{-1} for the exchange constant, as the relative population of the ground-state is 99% or higher for any energy difference greater than 45 cm^{-1}. The DFT calculations thus provide strong evidence that the exchange constant for $Mn^{II}-Mn^{III}$ interactions is ferromagnetic, with magnitude in the range 0.5 to 6.5 cm^{-1}. This is similar to exchange constants obtained for $Mn^{II}-Mn^{III}$ interactions in other complexes with metric parameters similar to those found for the $Mn^{II}-Mn^{III}$ pathways in **1**.[18,20,24]

Conclusions

The combination of azide and a chelating alkoxide-containing group has proved to be a useful route to new Mn^{III}-containing clusters with interesting structural and magnetic properties. The present work extends our previous results in this area, where a Mn_{25} cluster with azide and pdm^{2-}/$pdmH^{-}$ had been obtained, by identifying the products from the azide/hmpH, azide/$pdmH_2$/$thmeH_3$, and azide/$pdmH_2$/$teaH_3$ reaction systems, which are complexes **1**/**2**, **3**, and **4**, respectively. It is interesting that **1**−**3** are Mn_{10} clusters containing end-on bridging azide groups and bridging alkoxide arms of the chelate(s), and both are at the same $Mn^{II}_4Mn^{III}_6$ oxidation level. However, given these similarities, it is also interesting and indeed fascinating that they have such very different ground state S values, differing by a massive 22 units (44 unpaired electrons). Of course, this is an extreme example of something that otherwise is common, a change in the ground-state as a result of structural changes even when the same ligand types are involved. Nevertheless, the change in spin ground states in the present case is still noteworthy for its sheer magnitude. This is particularly true given that the couplings within the two types of molecules are likely not that different; almost certainly there is a mixture of both ferro- and antiferromagnetic exchange interactions within **3**, given that it still contains end-on bridging azide groups and alkoxide bridges that typically give ferromagnetic coupling, whereas **1** and **2** are completely ferromagnetically coupled. Complex **4** is the first mixed-chelate Mn_4 rhombus-like cluster and is also ferromagnetically coupled, containing bridging alkoxide arms from both types of chelate and terminal azide groups; it is again a mixed-valence ($Mn^{II}_2Mn^{III}_2$) with a large ground-state spin. As a consequence, slow magnetization relaxation phenomena were observed, indicative of SMM behavior.

The present work provides another clear example of the difficulty in predicting the ground states in high nuclearity Mn clusters. It will be interesting to determine as this work is extended to what extent N_3^-/alcohol-based ligands will continue to provide a route to new metal clusters, especially ones that might have interesting magnetic properties, and to what extent these are related to clusters provided by alcohol-based ligands alone.

Acknowledgment. This work was supported by NSF Grant CHE-0414555. The theoretical calculations were supported by an IBM Shared University Research grant to IU (T.O'B.). K.M.P. acknowledges funding from the Undergraduate Research Opportunities Program at IUPUI.

Supporting Information Available: Computational data obtained with ZILSH calculations for spin components of **1**, dc and ac magnetic data for complex **2** (PDF), and X-ray crystallographic files in CIF format for complexes **1**·MeCN, **2**·MeCN, **3**·$2H_2O$·MeCN, and **4**. This material is available free of charge via the Internet at http://pubs.acs.org.

IC800268Z